Vorticity Induced by a Moving Elliptic Belt

Calvin J. Ribbens, C.Y. Wang, Layne T. Watson
and Kevin A. Alexander

TR 89-35

Vorticity Induced by a Moving Elliptic Belt

Calvin J. Ribbens
Department of Computer Science
Virginia Polytechnic Institute & State University
Blacksburg, VA 24061

C.-Y. Wang
Departments of Mathematics and Mechanical Engineering
Michigan State University
East Lansing, MI 48824

Layne. T. Watson
Department of Computer Science
Virginia Polytechnic Institute & State University
Blacksburg, VA 24061

Kevin A. Alexander
Michelin MARC
P. O. Box 1987
Greenville, SC 29602

Abstract. The viscous flow inside an elliptic moving belt is studied using Newton's method on a Hermite collocation approximation. The streamlines and especially the vorticity distribution are found for Reynolds number up to 1000 and aspect ratio up to 5. For low Reynolds numbers vorticity diffuses from regions of high curvature. For high Reynolds numbers there exists a closed boundary layer and a core of constant vorticity. The core vorticity compares well with the estimation from the mean square law.

1. Introduction. Fluid flows with closed streamlines or recirculation occur in many instances, e.g., in the rear wakes behind bluff bodies, separated flows or inside bubbles and cavities. The simplest geometry which models recirculating flows is the circular boundary. Prescribed tangential velocities on the circle cause the interior fluid to rotate. For low Reynolds numbers, Kuwahara and Imai [1] studied the circular boundary by a perturbation about Stokes flow. They also used finite difference methods to integrate the equations for Reynolds numbers up to 128. For high Reynolds number flows, Batchelor [2] showed that the interior of a recirculating flow must be of constant vorticity. There is also a closed boundary layer surrounding and causing the interior rotation. For flows with zero pressure gradient along the boundary, Batchelor proved the important relationship that the mean square velocity along any streamline inside the boundary layer is constant.

High Reynolds number analytic solutions for the boundary layer on a circle (which has zero pressure gradient) were attempted by Squire [3] and Burggraf [4] using a perturbation about rigid rotation. Wood [5] noted that such Oseen approximation would not yield Batchelor's mean square law.

Wood [5] first considered the moving elliptic belt problem, the flow enclosed by an elliptic belt moving tangentially with constant speed. Perturbing about the small ellipticity, Wood found that for high Reynolds numbers the interior (constant) vorticity is inversely proportional to the square root of the area of the ellipse. Riley [6] and Haddon and Riley [7] studied analytically and by finite

differences the flow in an elliptic region, but with a very specific nonconstant boundary velocity. They found the core vorticity is indeed constant for high Reynolds numbers.

The present work considers the moving constant speed elliptic belt problem. We shall study in detail the flow and especially the vorticity distribution as ellipticity and Reynolds number are varied. For high Reynolds numbers the value of the core vorticity will be compared to the theoretical work of Wood [5] and an alternate estimate derived from the methods of Wood [5] and Mills [8].

2. Formulation. The two-dimensional steady Navier-Stokes equations are

$$u'u'_{x'} + v'u'_{y'} = -\frac{1}{\rho}p'_{x'} + \nu\left(u'_{x'x'} + u'_{y'y'}\right), \tag{1}$$

$$u'v'_{x'} + v'v'_{y'} = -\frac{1}{\rho}p'_{y'} + \nu\left(v'_{x'x'} + v'_{y'y'}\right), \tag{2}$$

$$u'_{x'} + v'_{y'} = 0. \tag{3}$$

Here u', v' are velocity components in the Cartesian x', y' directions, ρ is the density, p' is the pressure, and ν is the kinematic viscosity. The boundary conditions are that on the ellipse

$$\left(\frac{x'}{a}\right)^2 + \left(\frac{y'}{b}\right)^2 = 1$$

the velocity is tangent with a constant magnitude of U, and that the velocities are bounded inside the ellipse. We normalize all velocities by U, all lengths by b, the pressure by ρU^2 and drop primes. Define a stream function ψ by

$$u = \psi_y, \qquad v = -\psi_x. \tag{4}$$

The governing equations in the interior Ω of the ellipse become

$$\nabla^4\psi = R\left(\psi_y\nabla^2\psi_x - \psi_x\nabla^2\psi_y\right), \tag{5}$$

where ∇^2 is the Laplacian operator and R is the Reynolds number Ub/ν. The boundary conditions become, on the ellipse

$$x^2 + \lambda^2 y^2 = \lambda^2, \tag{6}$$

$$\psi = 0, \tag{7}$$

$$\psi_x^2 + \psi_y^2 = 1, \tag{8}$$

where the aspect ratio $\lambda \equiv a/b \geq 1$. The eccentricity of the ellipse is $\sqrt{1-\lambda^{-2}}$.

3. Numerical method. We apply a Newton-like iteration to Equation (5). It is well-known that if Newton's method converges to the root of a nonlinear equation, it does so rapidly. However, a good initial guess is usually needed for convergence to occur. For this problem, good initial guesses are available. For low Reynolds number ($R = 1$) we use as initial guess

$$\psi^{(0)}(x,y) = \left[x^2 + \lambda^2 y^2 - \lambda^2\right]/2. \tag{9}$$

If Ω is the unit disk (i.e., $\lambda = 1$), then $\psi^{(0)}$ exactly solves Equations (5–8). For a general ellipse ($\lambda \neq 1$), $\psi^{(0)}$ does not satisfy (8), but it does represent a smooth mapping of the known solution on the unit circle to an ellipse. A good initial guess, coupled with the fact that the size of the nonlinear term is relatively small when R is small, allows us to achieve rapid convergence for $R = 1$. Solutions for higher Reynolds number on a given ellipse are then computed by using as initial guess a solution for a slightly smaller R on the same ellipse.

To derive Newton's method for a nonlinear PDE such as Equation (5), we follow Rice and Boisvert [9], and consider the nonlinear operator

$$F(w) = \nabla^4 w - R(w_y \nabla^2 w_x - w_x \nabla^2 w_y). \tag{10}$$

Expanding F about some known function $w^{(0)}$, and keeping only the first two terms, we obtain

$$F(w) \approx F(w^{(0)}) + F'(w^{(0)})(w - w^{(0)}), \tag{11}$$

where F' is the Frechet derivative of F. $F'(w^{(0)})$ is an operator that depends on $w^{(0)}$, and in (11) is applied to the function $(w - w^{(0)})$. Setting the right side of Equation (11) to zero, we obtain the following iteration for approximately solving $F(w) = 0$: start with an initial guess $w^{(0)}$ for w, and for $i = 0, 1, 2, \ldots$, until some termination criterion is satisfied, solve

$$F'(w^{(i)})w^{(i+1)} = F'(w^{(i)})w^{(i)} - F(w^{(i)})$$

for $w^{(i+1)}$. The key observation is that $w^{(i)}$ is known and $F'(w^{(i)})$ is a linear elliptic operator. Thus, at each Newton step we must solve a linear problem for the next approximation $w^{(i+1)}$.

For the operator F defined by Equation (10), the Frechet derivative $F'(w)$ is found by considering

$$F(w + \delta) = \nabla^4(w + \delta) - R\left[(w + \delta)_y \nabla^2 (w + \delta)_x - (w + \delta)_x \nabla^2 (w + \delta)_y\right], \tag{12}$$

where δ is a small perturbation of w. If we keep only terms that are constant or linear in δ, we obtain

$$\begin{aligned} F(w + \delta) &\approx \nabla^4 w - R(w_y \nabla^2 w_x - w_x \nabla^2 w_y) + \nabla^4 \delta \\ &\qquad - R(w_y \nabla^2 \delta_x + \nabla^2 w_x \delta_y - w_x \nabla^2 \delta_y - \nabla^2 w_y \delta_x) \\ &= F(w) + F'(w)\delta, \end{aligned} \tag{13}$$

from which we conclude

$$F'(w^{(i)})w = \nabla^4 w - R\left(w_y^{(i)} \nabla^2 w_x + \nabla^2 w_x^{(i)} w_y - w_x^{(i)} \nabla^2 w_y - \nabla^2 w_y^{(i)} w_x\right). \tag{14}$$

After a similar linearization of the boundary condition (8), we obtain the following linear fourth order PDE to be solved at each iteration of Newton's method:

$$\begin{aligned} &\nabla^4 \psi - R\left(\psi_y^{(i)} \nabla^2 \psi_x + \nabla^2 \psi_x^{(i)} \psi_y - \psi_x^{(i)} \nabla^2 \psi_y - \nabla^2 \psi_y^{(i)} \psi_x\right) \\ &\quad = -R\left(\psi_y^{(i)} \nabla^2 \psi_x^{(i)} - \psi_x^{(i)} \nabla^2 \psi_y^{(i)}\right), \end{aligned} \tag{15}$$

subject to the boundary conditions

$$\psi = 0, \tag{16}$$

$$2\psi_x^{(i)}\psi_x + 2\psi_y^{(i)}\psi_y = 1 + \left(\psi_x^{(i)}\right)^2 + \left(\psi_y^{(i)}\right)^2. \tag{17}$$

In order to solve Equations (15–17) we rewrite (15) as a system of two second order equations

$$\nabla^2\phi - R\left(\psi_y^{(i)}\phi_x + \phi_x^{(i)}\psi_y - \psi_x^{(i)}\phi_y - \phi_y^{(i)}\psi_x\right) = -R\left(\psi_y^{(i)}\phi_x^{(i)} - \psi_x^{(i)}\phi_y^{(i)}\right), \tag{18}$$

$$\nabla^2\psi - \phi = 0, \tag{19}$$

where ϕ is the vorticity. We solve the coupled system (18) and (19) simultaneously. It is also convenient to transform the problem to a more natural but nonorthogonal coordinate system, in independent variables (r, θ), where

$$r = \sqrt{(x/\lambda)^2 + y^2}, \quad \theta = \tan^{-1}(\lambda y/x), \quad x = \lambda r\cos\theta, \quad y = r\sin\theta. \tag{20}$$

By symmetry, we may assume $\psi(r,\theta) = \psi(r,\theta+\pi)$. Thus, we only need to solve the transformed problem on the rectangle $\tilde{\Omega} = [0,1]\times[0,\pi]$. The boundary conditions imposed on $\partial\tilde{\Omega}$ are as follows:

Right side ($r = 1$): boundary conditions (16) and (17), transformed to the (r,θ) coordinate system.

Left side ($r = 0$): $\psi(0,\theta)$ must be a constant, since this side corresponds to a single point (the origin in the (x,y) coordinate system).

Bottom and top sides ($\theta = 0, \pi$): periodic boundary conditions (i.e., $\psi(r,0) = \psi(r,\pi)$).

We discretize Equations (15–17) (transformed to (r,θ) coordinates) using collocation with Hermite bicubic basis functions. Collocation is a flexible and general method that has been found to perform well on problems with difficult boundary conditions (see Dyksen, et al. [10, 11]). With this choice of basis functions, collocation is fourth order accurate on smooth problems (see Percell and Wheeler [12], and Prenter and Russell [13]). The boundary conditions on the right, top and bottom sides are handled easily by collocation. Special treatment is needed for the left side. It is straightforward to enforce the condition that ψ be constant along $r = 0$. In addition, one must enforce Equations (18) and (19) on the left side. Since the coefficients of the transformed PDE are undefined for $r = 0$, we impose the original PDE in Cartesian coordinates at the origin. Second-order finite difference approximations are used. The resulting equations (one for each of Equations (18) and (19)) may be included in the linear system produced by collocation since certain unknowns in that system correspond exactly to unknown function values at grid points near $r = 0$.

A modified version of the module HERMITE COLLOCATION (see Houstis, et al. [14]) is used to solve for $\psi^{(i+1)}$ and $\phi^{(i+1)}$ at each step of the Newton iteration. This software is available as part of the ELLPACK system described in Rice and Boisvert [9]. For the results reported below, the finest grid used has 33 grid lines in the r direction and 17 in the θ direction. The resulting discrete system has 4162 equations and unknowns. The grid spacing is uniform in θ. A modest amount of grid refinement in r is needed in order to get convergence and to accurately resolve the boundary layer along $r = 1$ for large R. For example, for $\lambda = 3$, 4 and 5, grid lines are placed at

$$r = 0,\ .05,\ .10,\ \ldots,\ .80,\ .817,\ .833,\ .85,\ .867,\ .883,\ .90,\ .91,\ .92,\ \ldots,\ .99,\ 1.$$

For each ellipse, solutions are obtained for Reynolds number

$$R = 1,\ 5,\ 10,\ 25,\ 50,\ 75,\ 100,\ 150,\ 200,\ 250,\ 300,\ 400,\ \ldots,\ 1000.$$

The Newton iteration is stopped when the maximum relative change in ψ at the grid points falls below 10^{-7}. Convergence typically occurred in less than 5 Newton iterations. The computations were done in double precision on a Sequent Symmetry S81 with 10 processors and Weitek 1167 floating point coprocessors, using the *fortran* compiler.

4. Results. Results are obtained for $\lambda = 1$ to 5 (elliptic eccentricity 0 to 0.9798). The Reynolds number is varied from 1 to 1000. Typical streamlines are shown in Figs. (1, 2) for two different aspect ratios λ. The increase in Reynolds number does not alter the streamlines much. Since the boundary speed is always positive, one single recirculation cell will be observed for all λ and R.

The vorticity picture is quite different. Fig. (3) shows the constant vorticity lines for the 2:1 ellipse. At low Reynolds numbers vorticity is concentrated at the vertices of the major axis. As Reynolds number is increased, vorticity changes become confined in a thin layer near the boundary. Note also that vorticity is not symmetrical with respect to the axes x, y. This is clearly shown for the larger Reynolds numbers where convection is important. Since the belt is moving in a clockwise sense, vorticity is transported downstream. The detailed vorticity structure is shown in Fig. (4) for $R = 100$ and Fig. (5) for $R = 1000$. Fig. (6) shows the long ellipse with $\lambda = 5$. The detailed structures for $R = 100$ and $R = 1000$ are shown in Figs. (7, 8).

In order to investigate the constancy of vorticity at high Reynolds numbers, we plotted $\phi = \nabla^2\psi$ along radial lines from the origin for $R = 1000$. For the 2:1 ellipse Fig. (9) clearly shows vorticity is constant for much of the interior. The boundary layer near $r = 1$ is evident. The vorticity distribution on the elliptic boundary (or shear stress) is not constant, however (Fig. (10)). It is doubly periodic with maximums near $\theta = 20°$ and $200°$. The minimums are near $\theta = 110°$ and $290°$. Negative shear stress here does not mean separation since the boundary velocity is not zero. Similar results for $\lambda = 5$ (Figs. (11, 12)) show ellipticity does not affect the constancy of the interior vorticity. However, the shear on the boundary is less smooth.

If the interior vorticity is constant for high Reynolds numbers, it can be represented by its value at the origin. Fig. (13) shows this value rises to a plateau when Reynolds number is increased to about 100, then a very slow, almost imperceptible, increase from $R = 100$ to 1000. The interior vorticity is almost independent of R at high Reynolds numbers.

5. Comparison with theory at high Reynolds numbers. The boundary layer equation in von Mises form is

$$\frac{\partial u^2}{\partial s} = \frac{dV^2}{ds} + \nu u \frac{\partial^2 u^2}{\partial \psi^2}. \tag{21}$$

Here s is the arc length along the boundary and $V(s)$ is the interior velocity evaluated at the boundary. Following Wood [5] and Mills [8], Eq. (21) is linearized to

$$\frac{\partial u^2}{\partial s} = \frac{dV^2}{ds} + \nu \bar{U} \frac{\partial^2 u^2}{\partial \psi^2}, \tag{22}$$

where $\bar{U}$ is the constant root mean squared value of the boundary velocity $U(s)$. Integrating Eq. (22) along any closed streamline in the boundary layer yields

$$\oint \frac{\partial^2 u^2}{\partial \psi^2} ds = 0. \tag{23}$$

One further integration gives the mean squared law

$$\oint u^2 \, ds = \text{constant} = \oint V^2 \, ds. \tag{24}$$

On the boundary $u = U$ and thus

$$\oint U^2 \, ds = \oint V^2 \, ds. \tag{25}$$

Table 1.
Comparison of vorticity at origin with analytical predictions.

λ	Numerical $\phi(0,0)$ at $R = 1000$	Analytical Eq. (29)	Analytical Wood [5]
1.0	2.000	2.000	2.000
1.1	1.907	1.909	1.907
1.3	1.755	1.770	1.754
1.5	1.641	1.668	1.633
1.7	1.554	1.593	1.534
2.0	1.462	1.510	1.414
3.0	1.297	1.371	1.155
4.0	1.237	1.314	1.000
5.0	1.209	1.285	0.894

For the present problem $U = 1$. The inviscid rotational flow of the core is

$$\psi = \frac{\phi_0}{2(1+\lambda^2)}(x^2 + \lambda^2 y^2 - \lambda^2), \tag{26}$$

where ϕ_0 is the constant core vorticity. Thus

$$V^2 = (\psi_x)^2 + (\psi_y)^2 = \frac{\phi_0^2}{(1+\lambda^2)^2}(x^2 + \lambda^4 y^2). \tag{27}$$

In terms of our (r, θ) coordinates, on $r = 1$

$$ds = \sqrt{(dx)^2 + (dy)^2} = \sqrt{\lambda^2 \sin^2\theta + \cos^2\theta}\, d\theta. \tag{28}$$

Eq. (25) becomes

$$\phi_0 = \left(\lambda + \frac{1}{\lambda}\right)\sqrt{\frac{I_1}{I_2}}, \tag{29}$$

where

$$I_1 = \oint (\lambda^2 \sin^2\theta + \cos^2\theta)^{1/2} d\theta, \tag{30}$$

$$I_2 = \oint (\lambda^2 \sin^2\theta + \cos^2\theta)^{3/2} d\theta. \tag{31}$$

For given λ, ϕ_0 can be evaluated by numerical quadrature. The results are shown in Table 1. We see that our approximate formula Eq. (29) is within 6% of the numerical values. In contrast, Wood's [5] $(\text{area})^{-1/2}$ rule greatly underestimates the interior vorticity, especially for the higher aspect ratios.

6. Conclusions. Using a combination of Newton's method and Hermite collocation we calculated completely the flow due to a moving elliptic belt. Streamline and vorticity plots were obtained for the first time. Results for Reynolds number larger than 1000 can be obtained, although with minimal gain in information. Also turbulence may set in for larger Reynolds numbers.

We find that for low Reynolds numbers vorticity diffuses from regions of high curvature of the boundary. As Reynolds number is increased, convection causes the vorticity to spread in a continuous layer near the boundary. The interior vorticity becomes constant and independent of the Reynolds number. For our problem, such a state occurs for R larger than about 100. Even though a pressure gradient exists along the boundary, we find the mean square law still holds even for ellipses with high aspect ratios.

We emphasize that it is very difficult to discern the character of the flow by studying the streamlines alone. For example, there seems to be little change in streamlines for $R = 1$ or $R = 1000$ (Fig. (1)), but the vorticity picture is entirely different (Figs. (3a), (3d)). We also note the fallacy of modelling high Reynolds number recirculating flows with a concentrated vortex (e.g., Bryson [15]). Although the streamlines are closed, there is no evidence vorticity is concentrated in the interior. We find the interior vorticity is evenly spread, and its magnitude is quite low compared to boundary vorticity.

7. Acknowledgement. The work of C. J. Ribbens was supported in part by DOE grant DE-FG05-88ER25068, and the work of L. T. Watson was supported in part by AFOSR Grant 89–0497 and DOE grant DE-FG05-88ER25068.

8. References.

[1] K. Kuwahara and I. Imai, "Steady viscous flow with a circular boundary," *Phys. Fluids Suppl.*, **II**, 94–101 (1969).

[2] G. K. Batchelor, "On steady laminar flow with closed streamlines at large Reynolds number," *J. Fluid Mech.*, **1**, 177–190 (1956).

[3] H. B. Squire, "Note on the motion inside a region of recirculation (cavity flow)," *J. Roy. Aero. Soc.*, **60**, 203–205 (1956).

[4] O. R. Burggraf, "Analytical and numerical studies of the structure of steady separated flow," *J. Fluid Mech.*, **24**, 113–151 (1966).

[5] W. W. Wood, "Boundary layers whose streamlines are closed," *J. Fluid Mech.*, **2**, 77–87 (1957).

[6] N. Riley, "High Reynolds number flows with closed streamlines," *J. Eng. Math.*, **15**, 15–27 (1981).

[7] E. W. Haddon and N. Riley, "On flows with closed streamlines," *J. Eng. Math.*, **19**, 233–246 (1985).

[8] R. D. Mills, "On the closed motion of a fluid in a square cavity," *J. Roy. Aero. Soc.*, **69**, 116–120 (1965).

[9] J. R. Rice and R. F. Boisvert, *Solving Elliptic Problems Using ELLPACK*, Springer-Verlag, New York, (1985).

[10] W.R. Dyksen, E.N. Houstis, R.E. Lynch and J.R. Rice, "The performance of the collocation and Galerkin methods with Hermite bi-cubics," *SIAM J. Numer. Anal.*, **21**, 695–715 (1984).

[11] W.R. Dyksen, C.J. Ribbens and J.R. Rice, "The performance of numerical methods for elliptic problems with mixed boundary conditions," *Num. Meth. PDE*, 4, 347–361 (1988).

[12] P. Percell and M.F. Wheeler, "A C^1 finite collocation method for elliptic equations," *SIAM J. Numer. Anal.*, **17**, 605–622 (1980).

[13] P.M. Prenter and R.D. Russell, "Orthogonal collocation for elliptic partial differential equations," *SIAM J. Numer. Anal.*, **13**, 923–939 (1976).

[14] E.N. Houstis, W.F. Mitchell and J.R. Rice, "Collocation software for second-order elliptical partial differential equations," *ACM Trans. Math. Software*, **11**, 379–412 (1985).

[15] A. E. Bryson, "Symmetric vortex separation on circular cylinders and cones," *J. Appl. Mech.*, **26**, 643–648 (1959).

Figure Captions

Figure 1. Streamlines for $\lambda = 2$, top $R = 1$, bottom $R = 1000$, $\Delta\psi = 0.05$.

Figure 2. Streamlines for $\lambda = 5$, top $R = 1$, bottom $R = 1000$, $\Delta\psi = 0.05$.

Figure 3. Constant vorticity lines for $\lambda = 2$. (a) $R = 1$, (b) $R = 10$, (c) $R = 100$, (d) $R = 1000$. $\Delta\phi = 0.5$.

Figure 4. Constant vorticity lines for $\lambda = 2$, detail for $R = 100$, $\Delta\phi = 0.5$.

Figure 5. Constant vorticity lines for $\lambda = 2$, detail for $R = 1000$, $\Delta\phi = 1.0$.

Figure 6. Constant vorticity lines for $\lambda = 5$. (a) $R = 1$, (b) $R = 10$, (c) $R = 100$, (d) $R = 1000$. $\Delta\phi = 1.0$.

Figure 7. Constant vorticity lines for $\lambda = 5$, detail for $R = 100$, $\Delta\phi = 1.0$.

Figure 8. Constant vorticity lines for $\lambda = 5$, detail for $R = 1000$, $\Delta\phi = 1.0$.

Figure 9. Vorticity distribution along a ray, $\lambda = 2$, $R = 1000$.

Figure 10. Vorticity distribution along the boundary, $\lambda = 2$, $R = 1000$.

Figure 11. Vorticity distribution along a ray, $\lambda = 5$, $R = 1000$.

Figure 12. Vorticity distribution along the boundary, $\lambda = 5$, $R = 1000$.

Figure 13. Vorticity at origin as a function of Reynolds number. (a) $\lambda = 2$, (b) $\lambda = 5$.

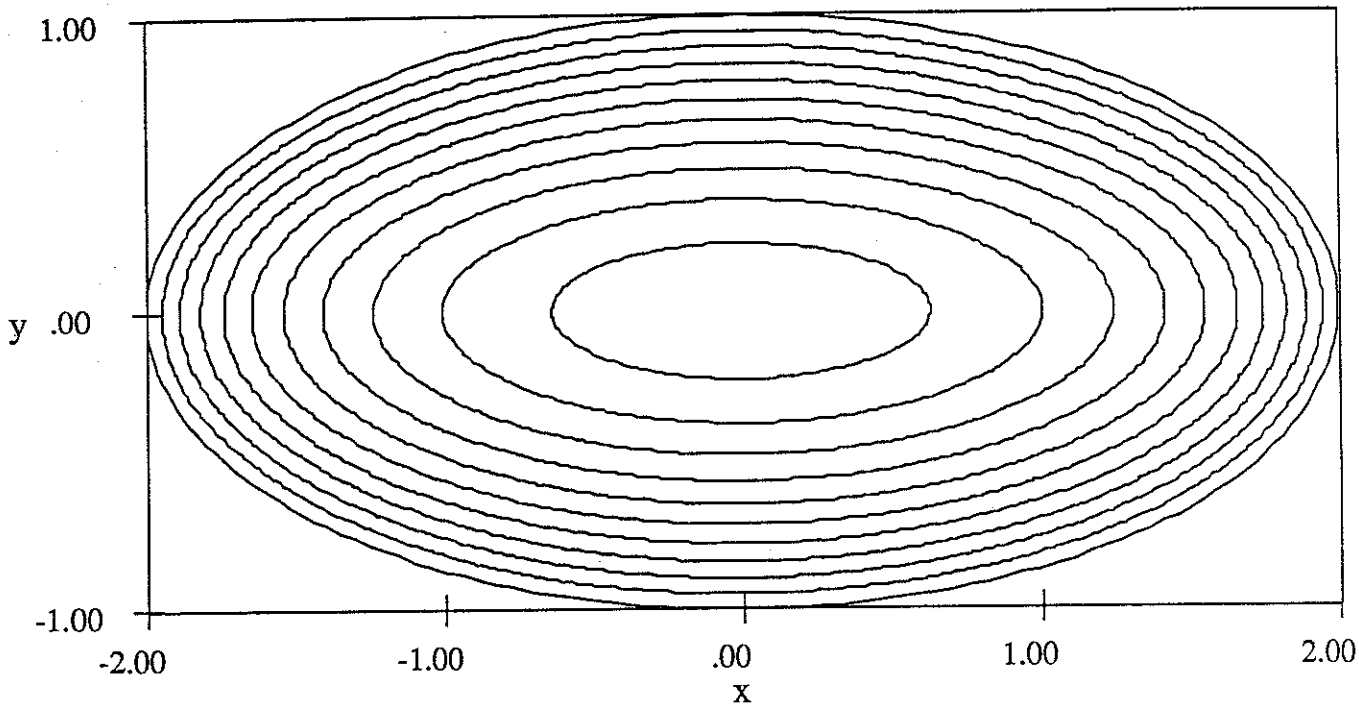

Figure 1 top

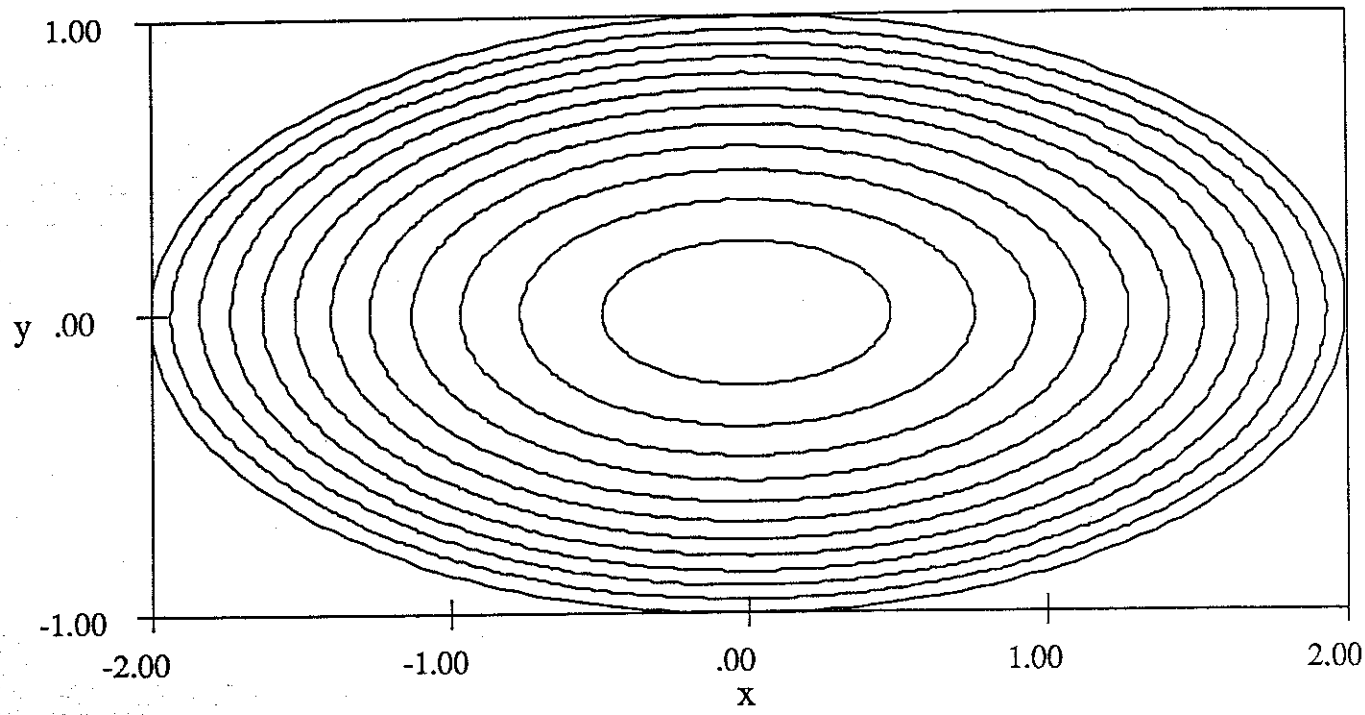

Figure 1 bottom

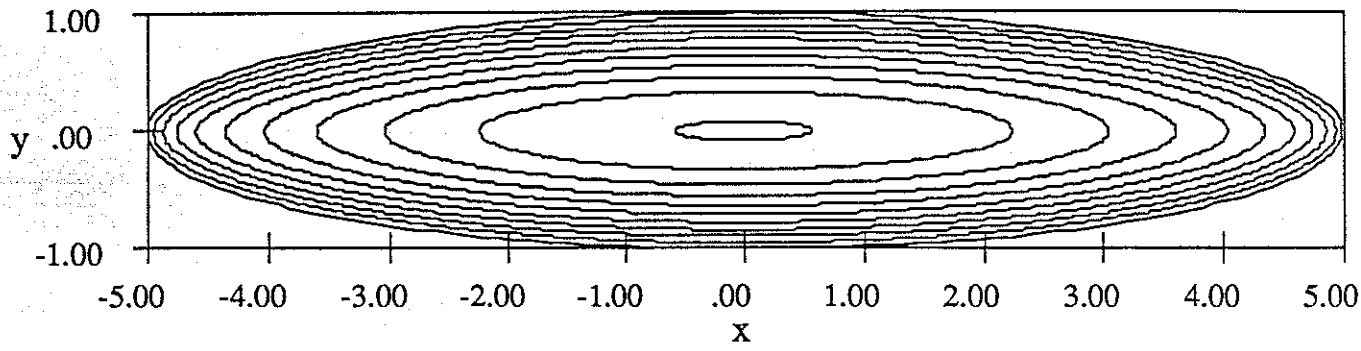

Line 2 top

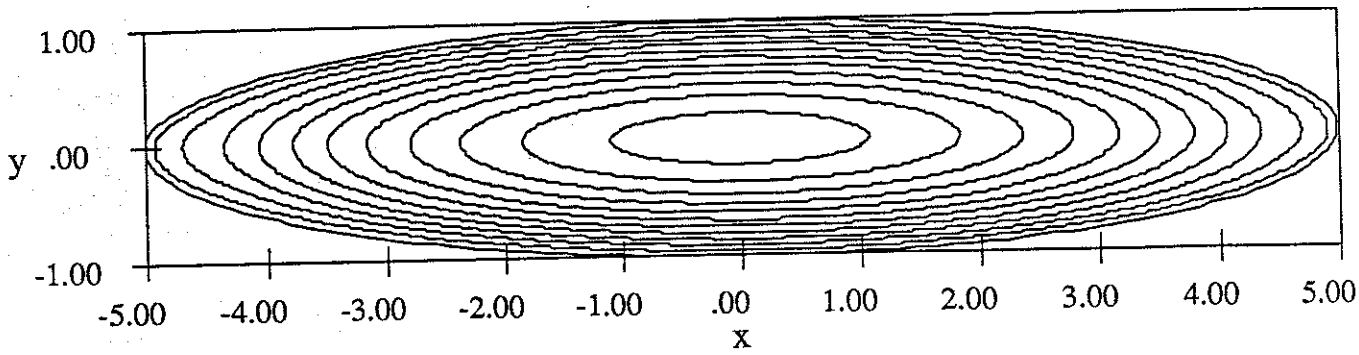
1.00
y .00
-1.00
-5.00
-4.00
-3.00
-2.00
-1.00
.00
1.00
2.00
3.00
4.00
5.00
x

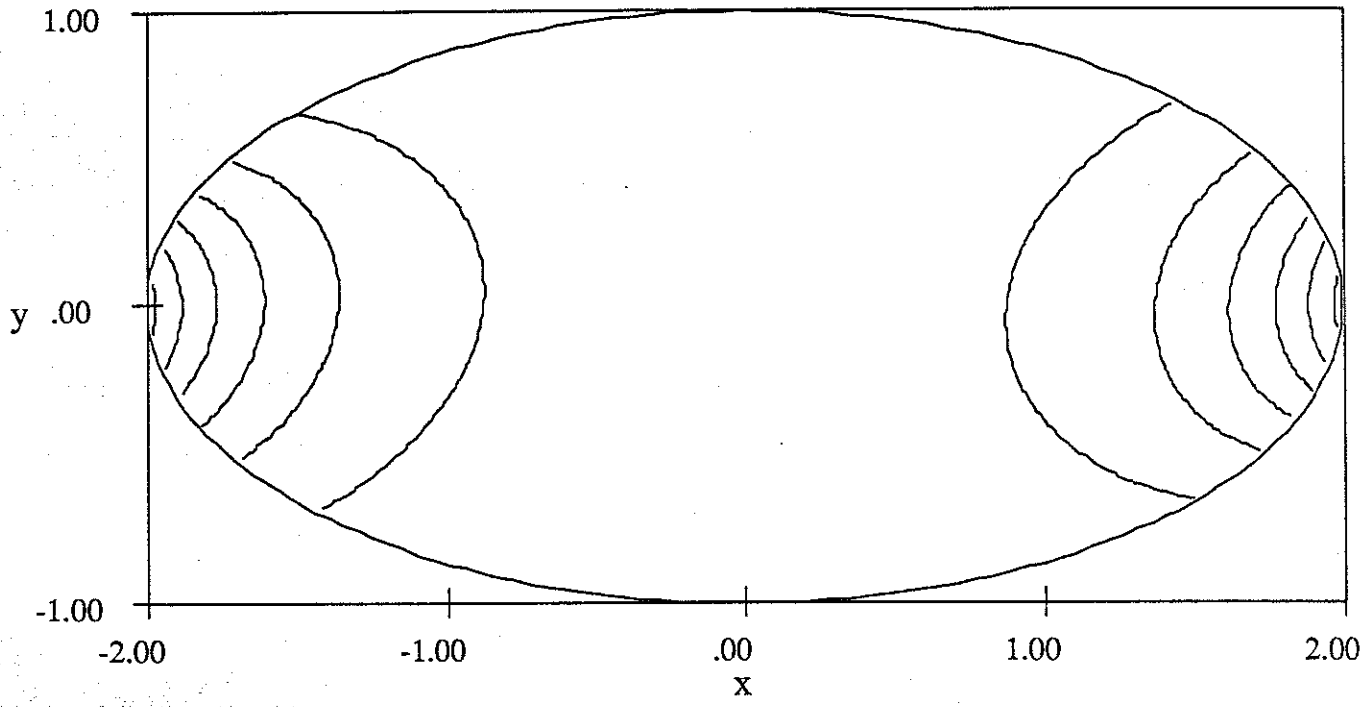
1.00
y .00
-1.00
-2.00
-1.00
.00
1.00
2.00
x

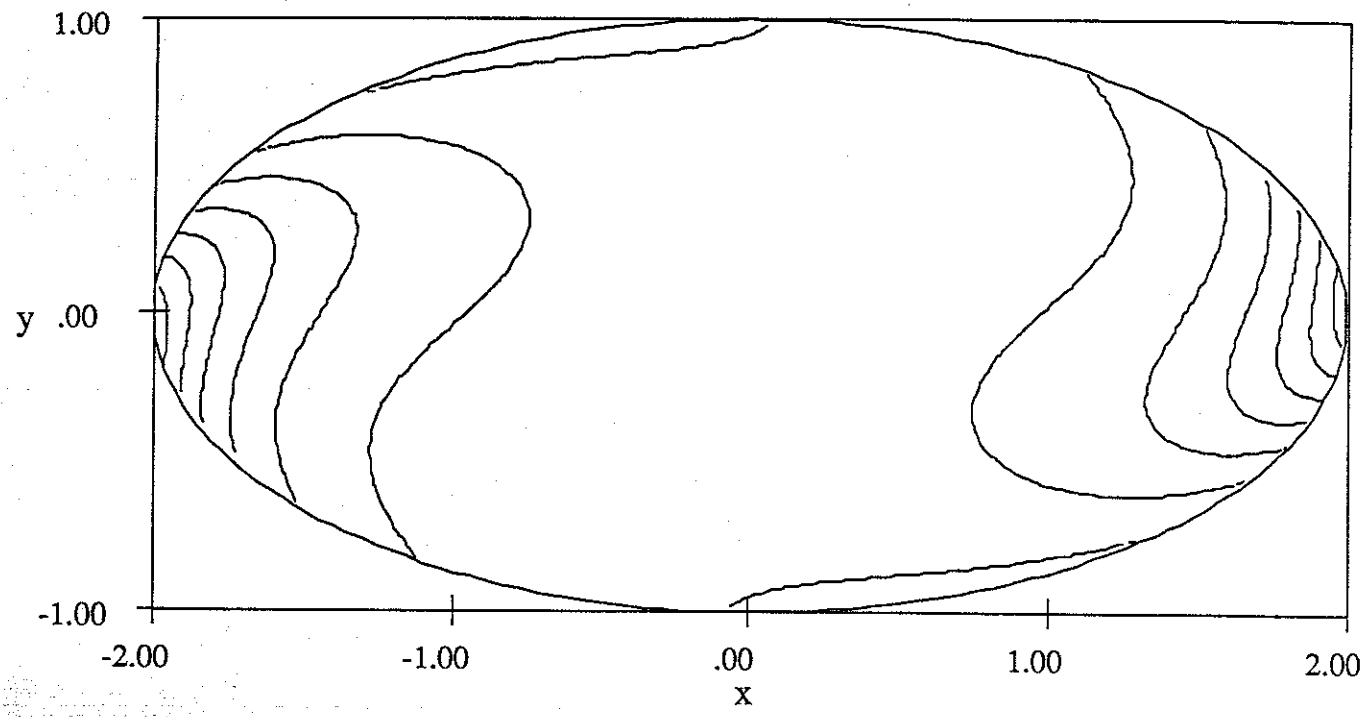
1.00
y .00
-1.00
-2.00
-1.00
.00
1.00
2.00
x

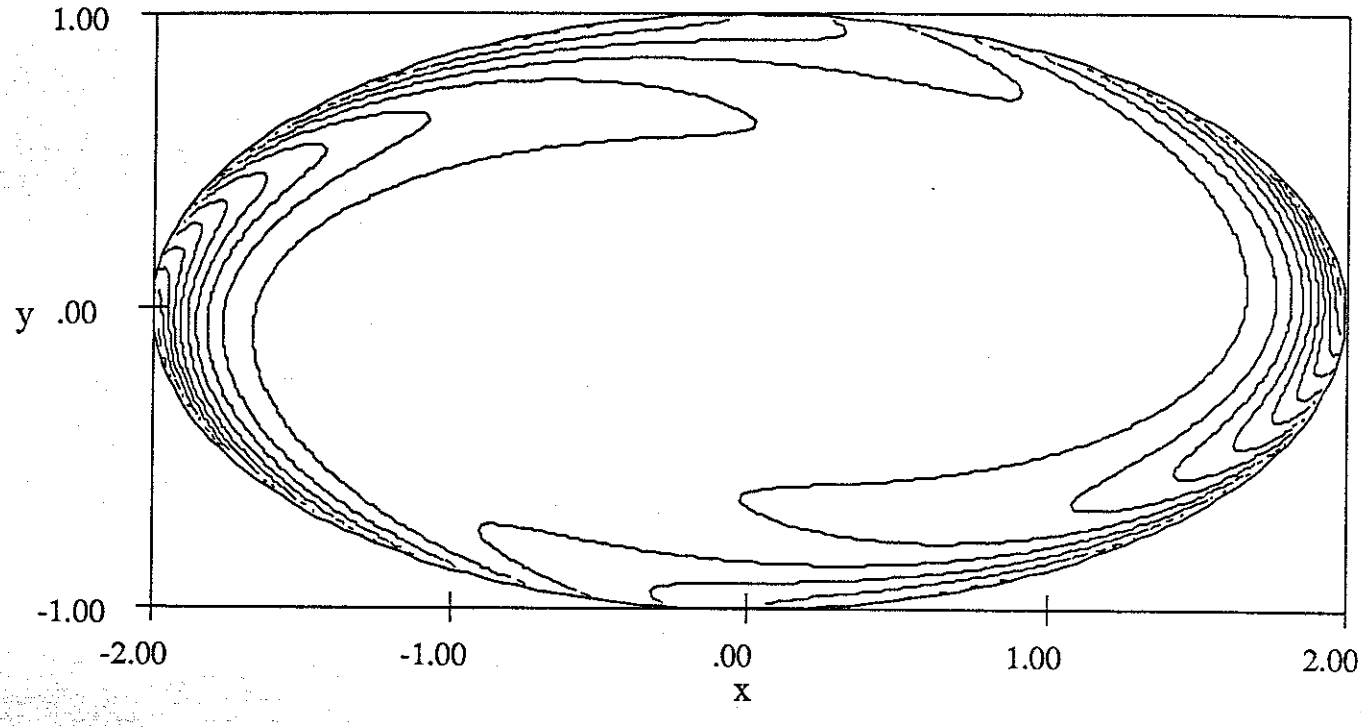
1.00
y .00
-1.00
-2.00
-1.00
.00
1.00
2.00
x

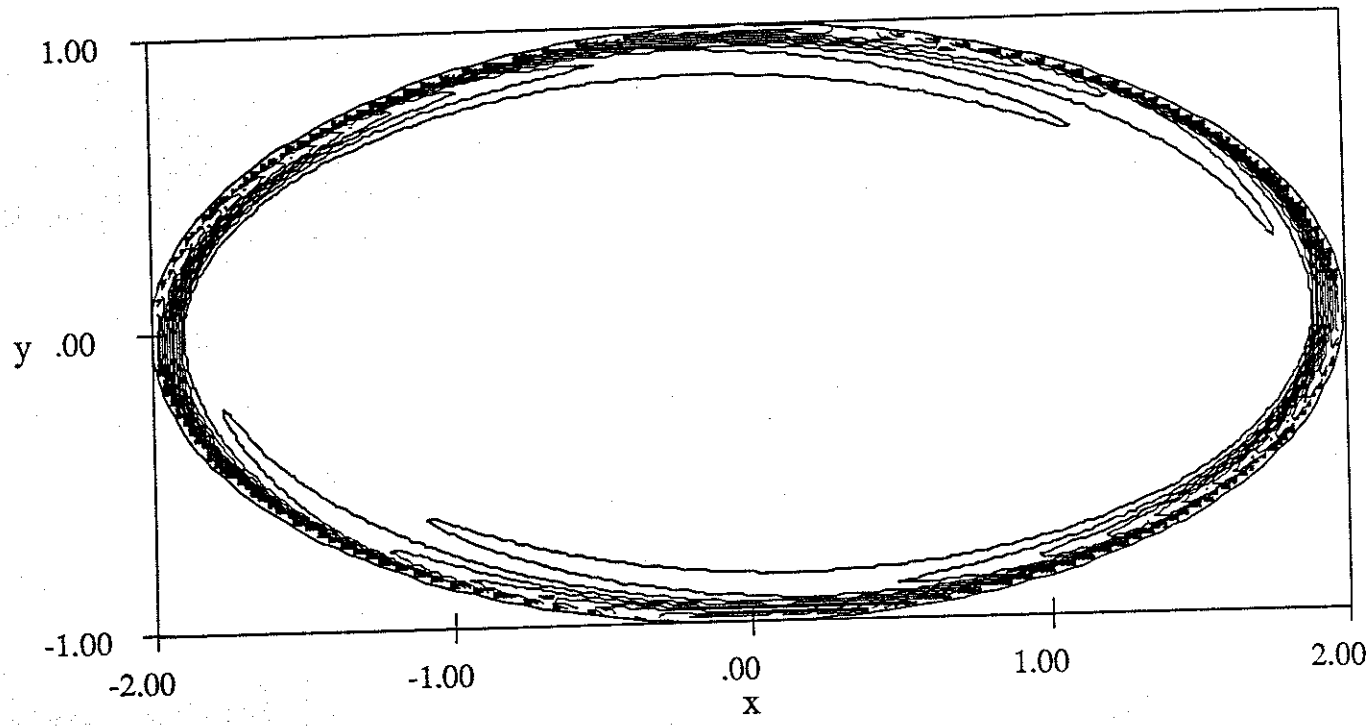

3(d)

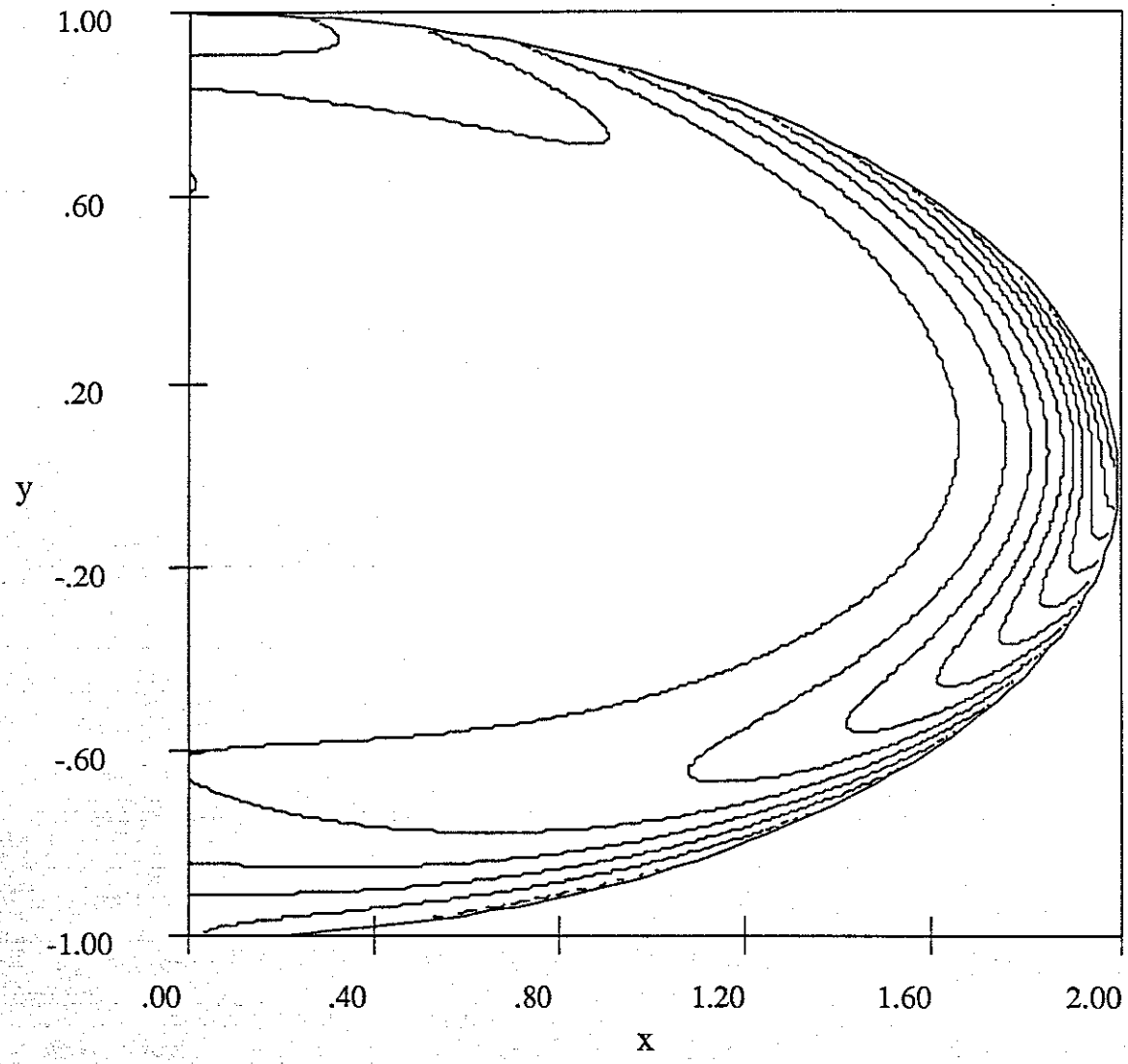
1.00
.60
.20
y
-.20
-.60
-1.00
.00
.40
.80
1.20
1.60
2.00
x

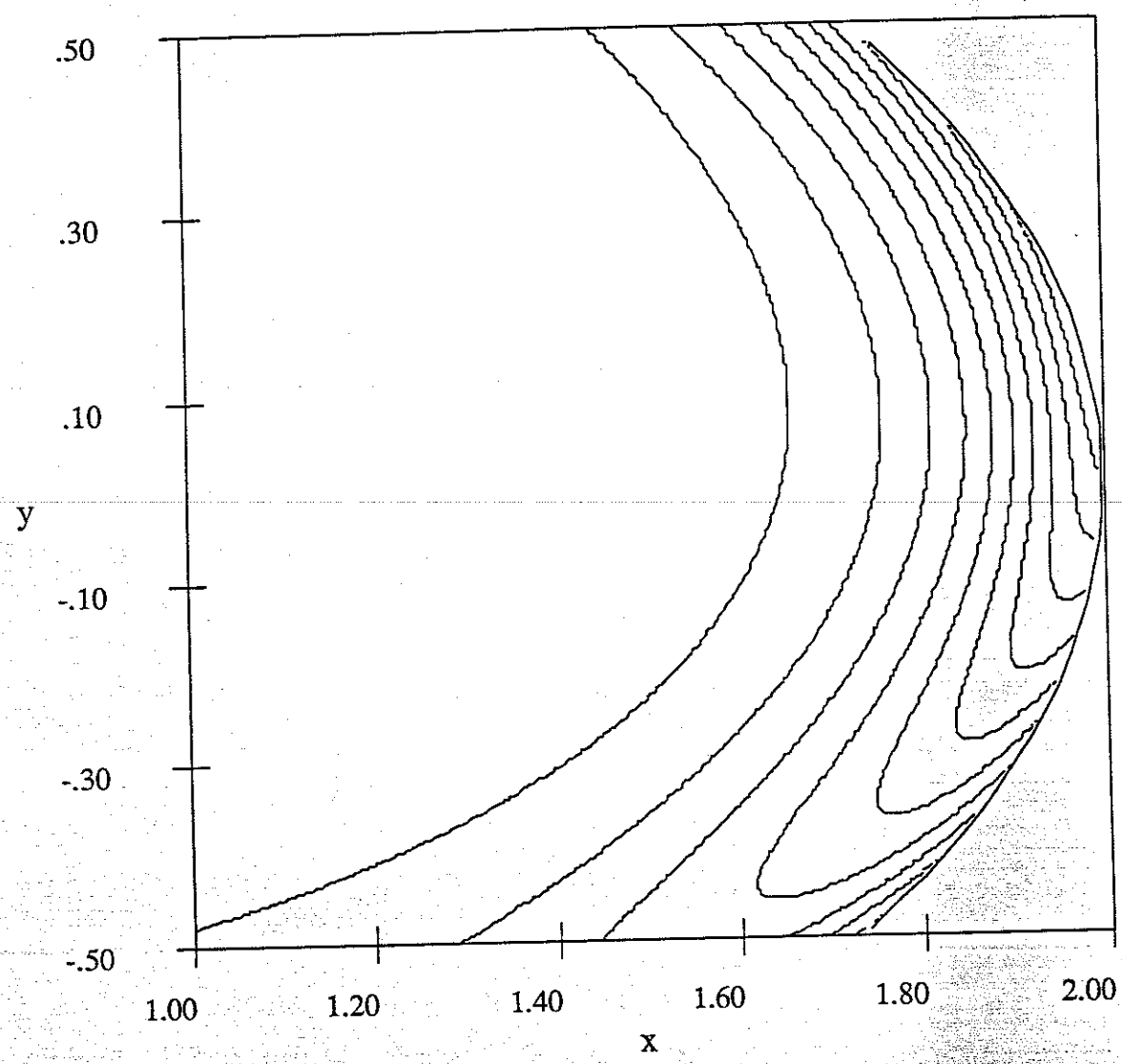
.50
.30
.10
-.10
-.30
-.50
y
1.00
1.20
1.40
1.60
1.80
2.00
x

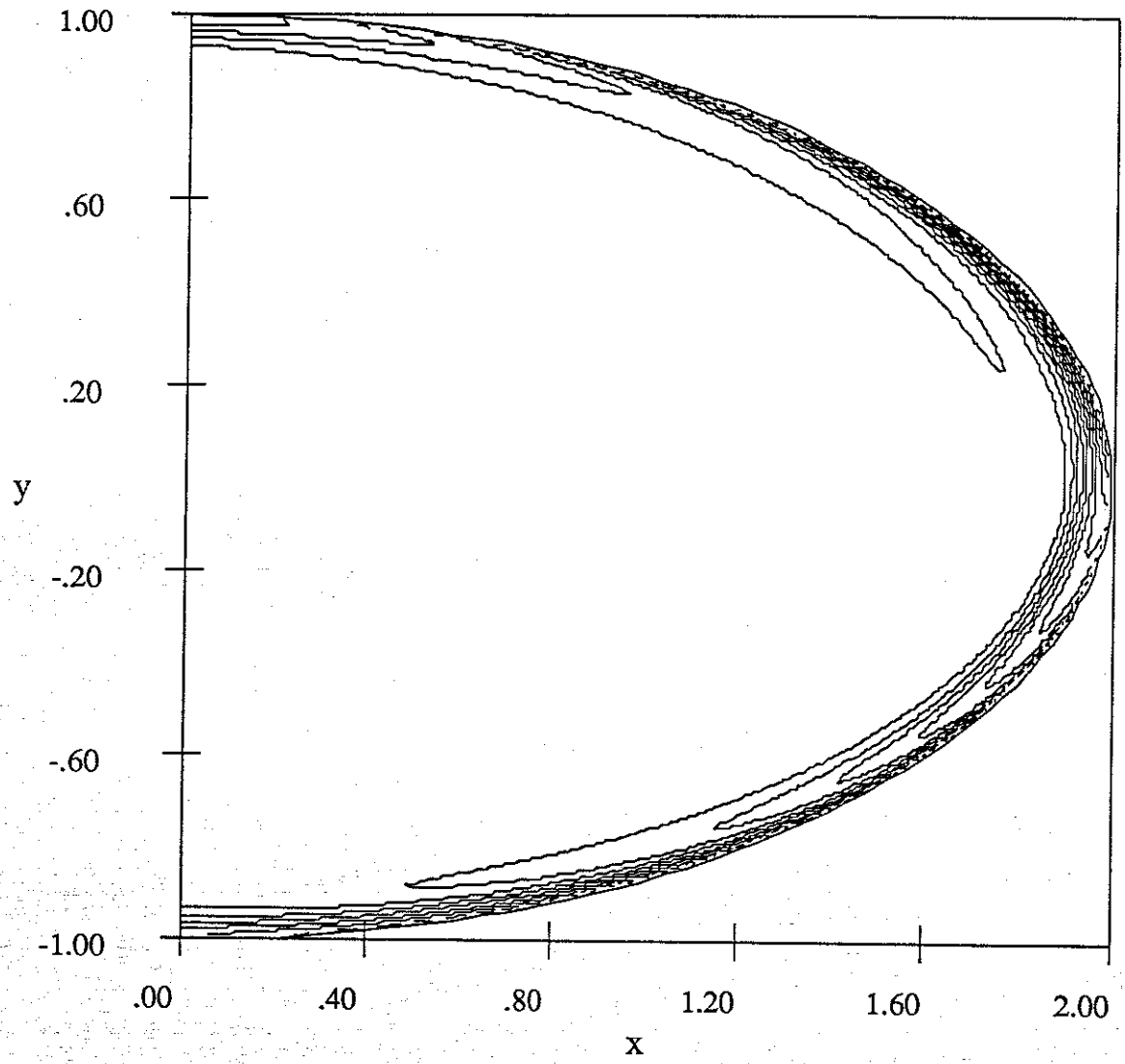
1.00
.60
.20
y
-.20
-.60
-1.00
.00
.40
.80
1.20
1.60
2.00
x

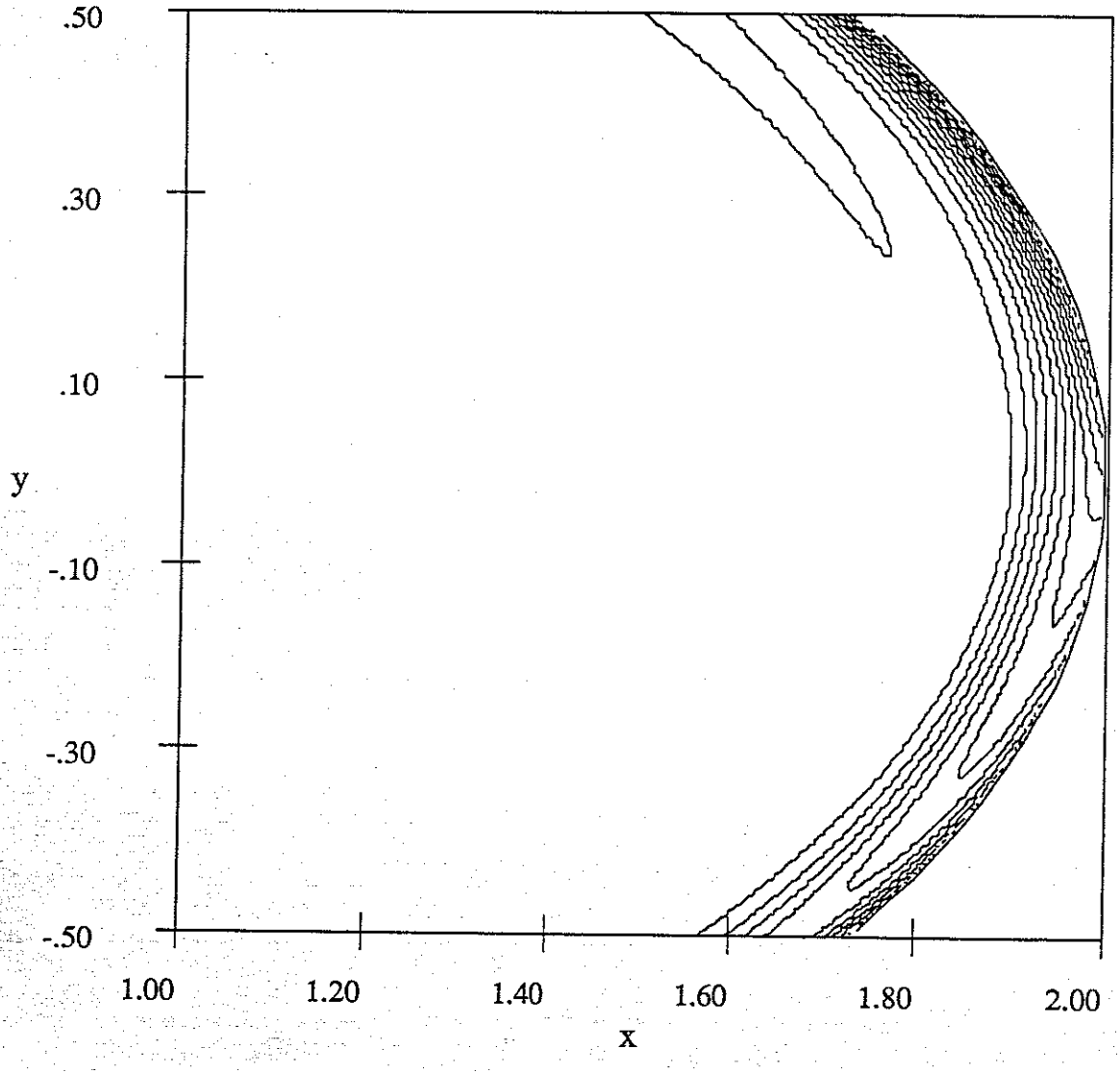
.50
.30
.10
-.10
-.30
-.50
y
1.00
1.20
1.40
1.60
1.80
2.00
x

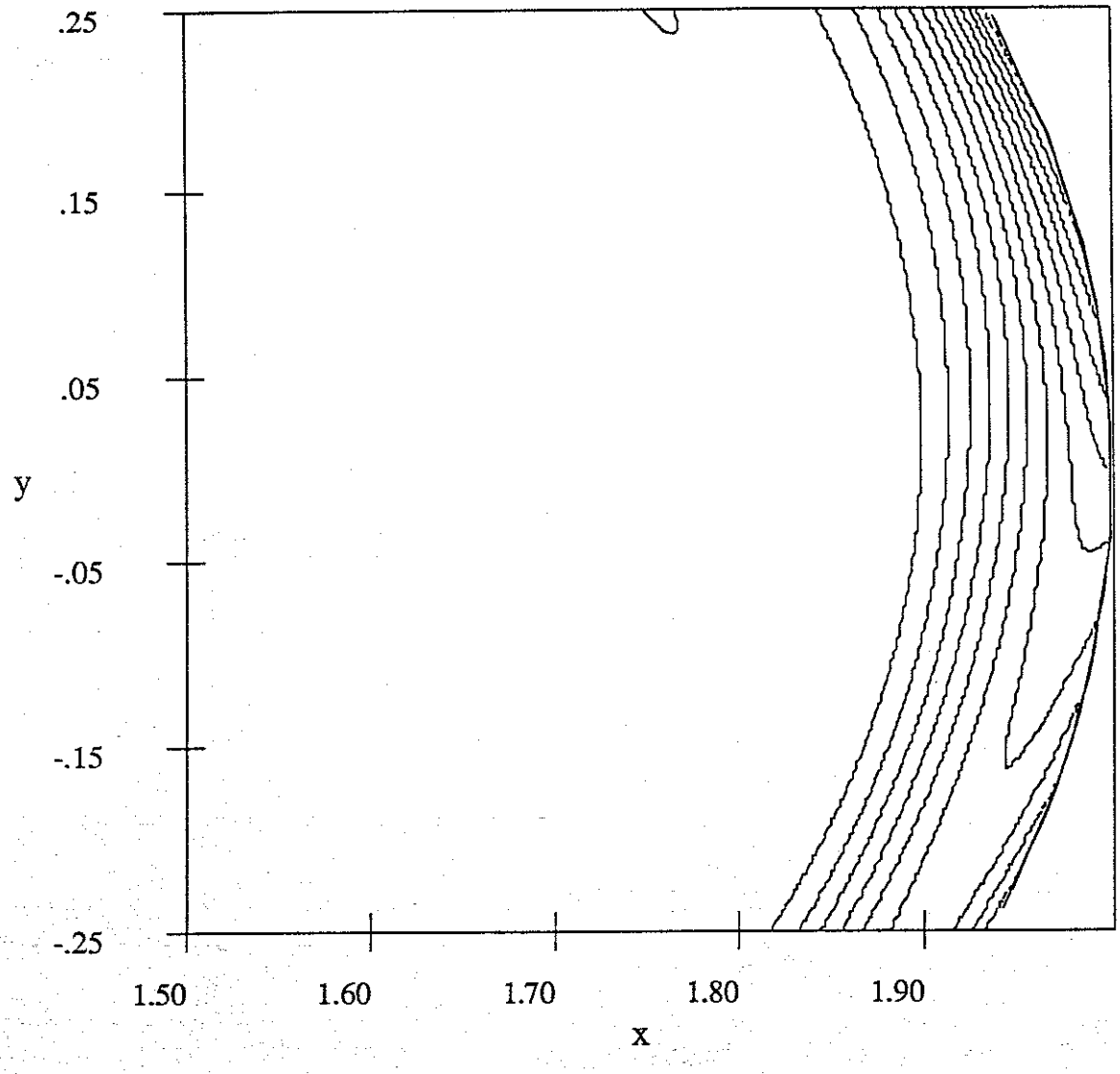
.25
.15
.05
-.05
-.15
-.25
y
1.50
1.60
1.70
1.80
1.90
x

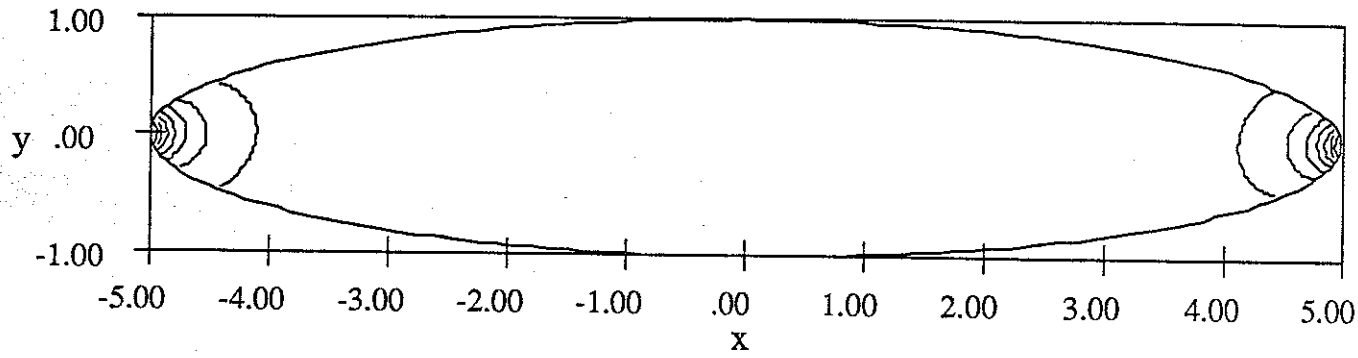
1.00
y .00
-1.00
-5.00
-4.00
-3.00
-2.00
-1.00
.00
1.00
2.00
3.00
4.00
5.00
x

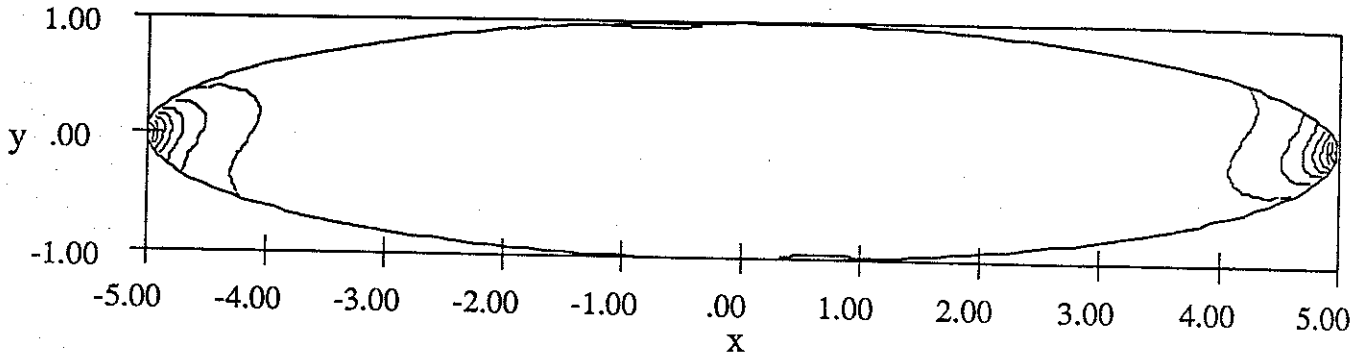
1.00
y .00
-1.00
-5.00
-4.00
-3.00
-2.00
-1.00
.00
1.00
2.00
3.00
4.00
5.00
x

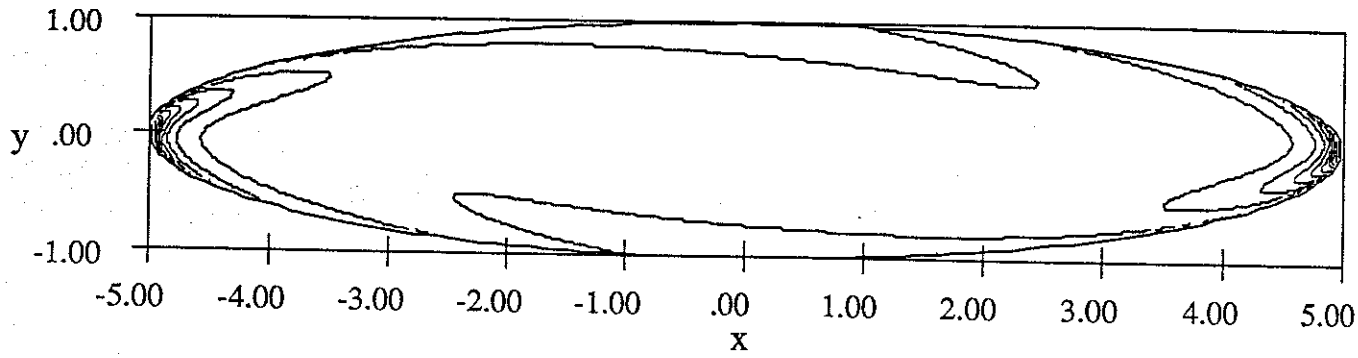

6(c)

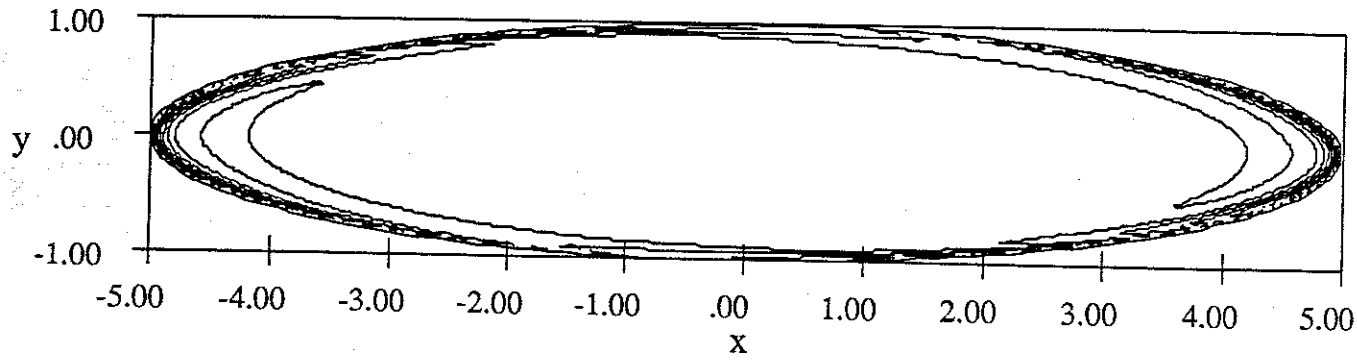
1.00
y .00
-1.00
-5.00
-4.00
-3.00
-2.00
-1.00
.00
1.00
2.00
3.00
4.00
5.00
x

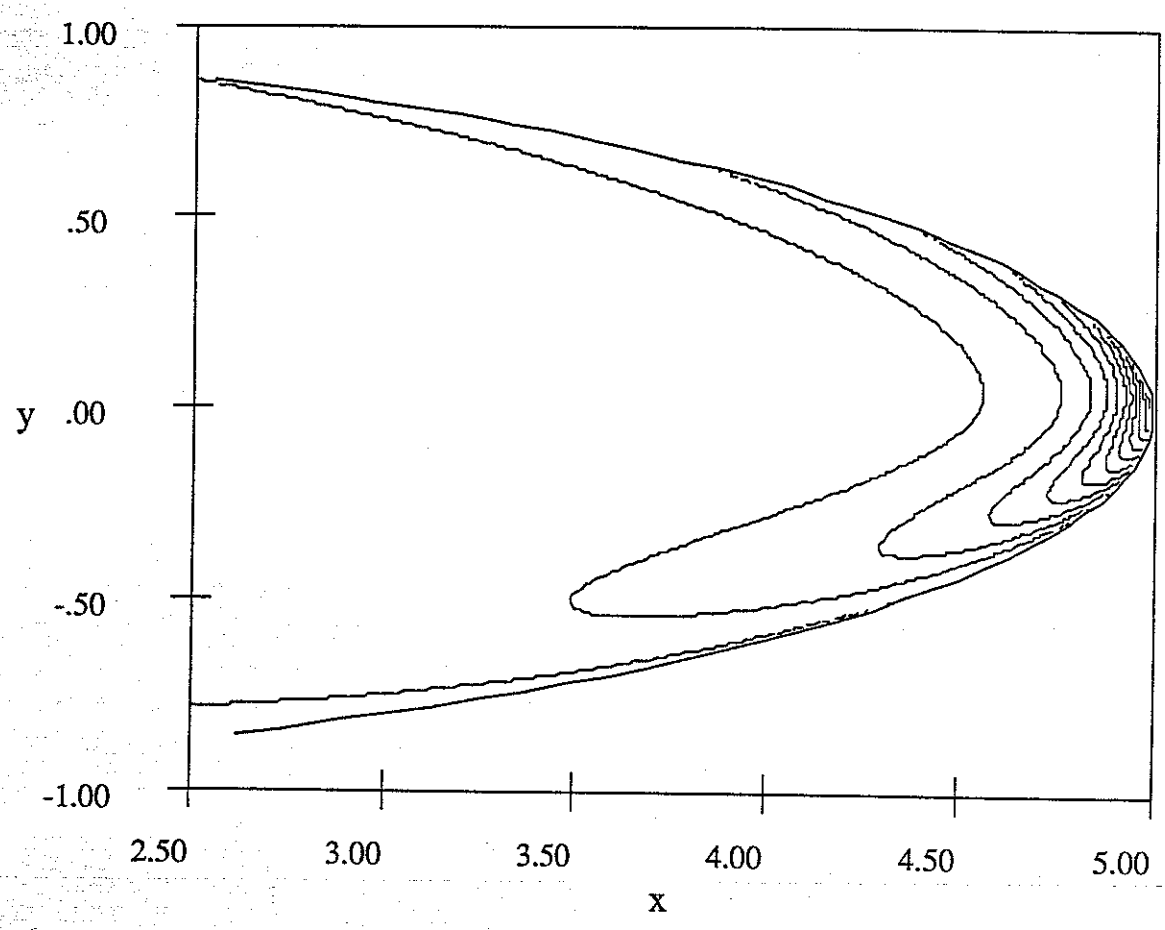
1.00
.50
y .00
-.50
-1.00
2.50
3.00
3.50
4.00
4.50
5.00
x

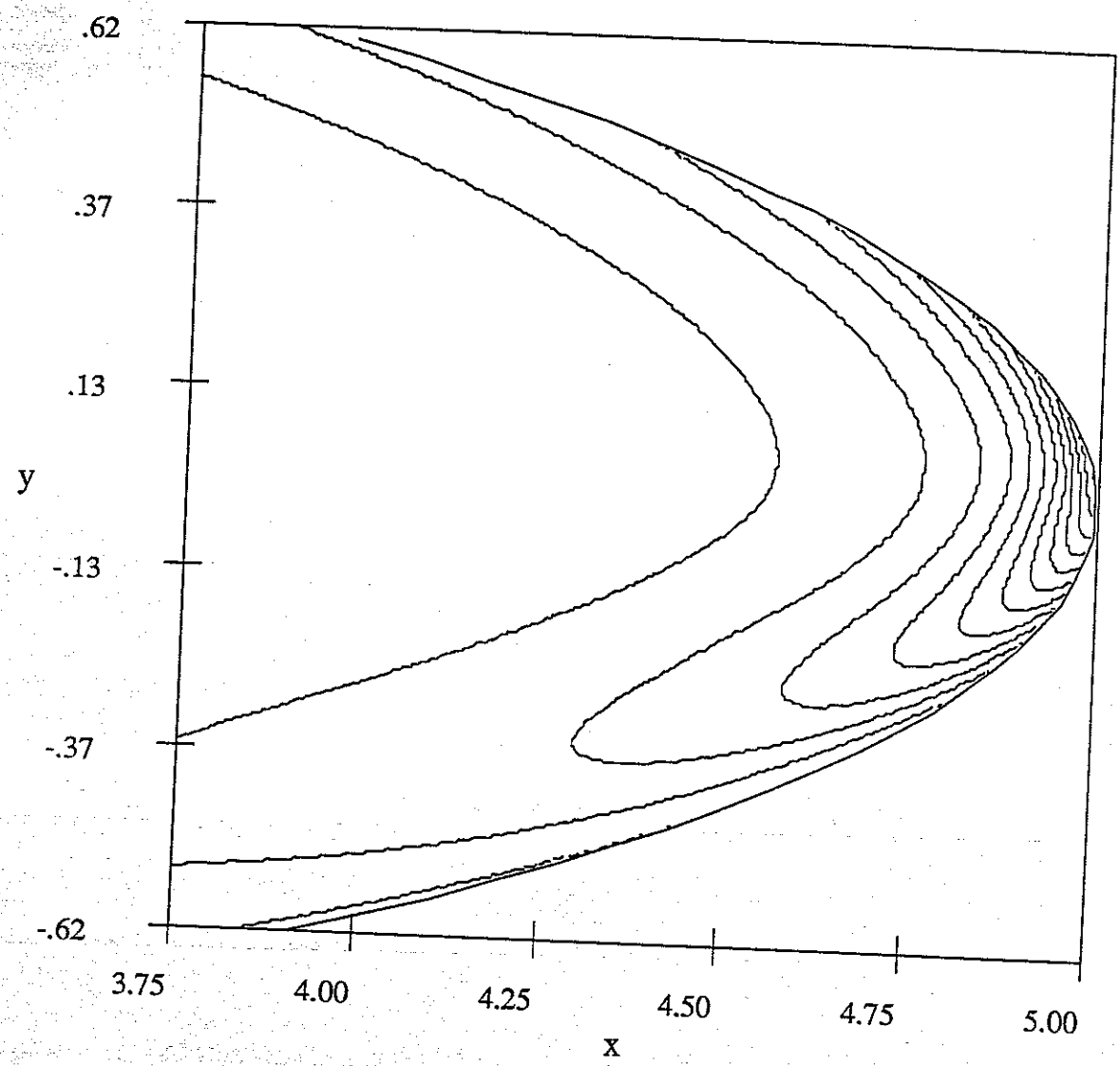
.62
.37
.13
y
-.13
-.37
-.62
3.75
4.00
4.25
4.50
4.75
5.00
x

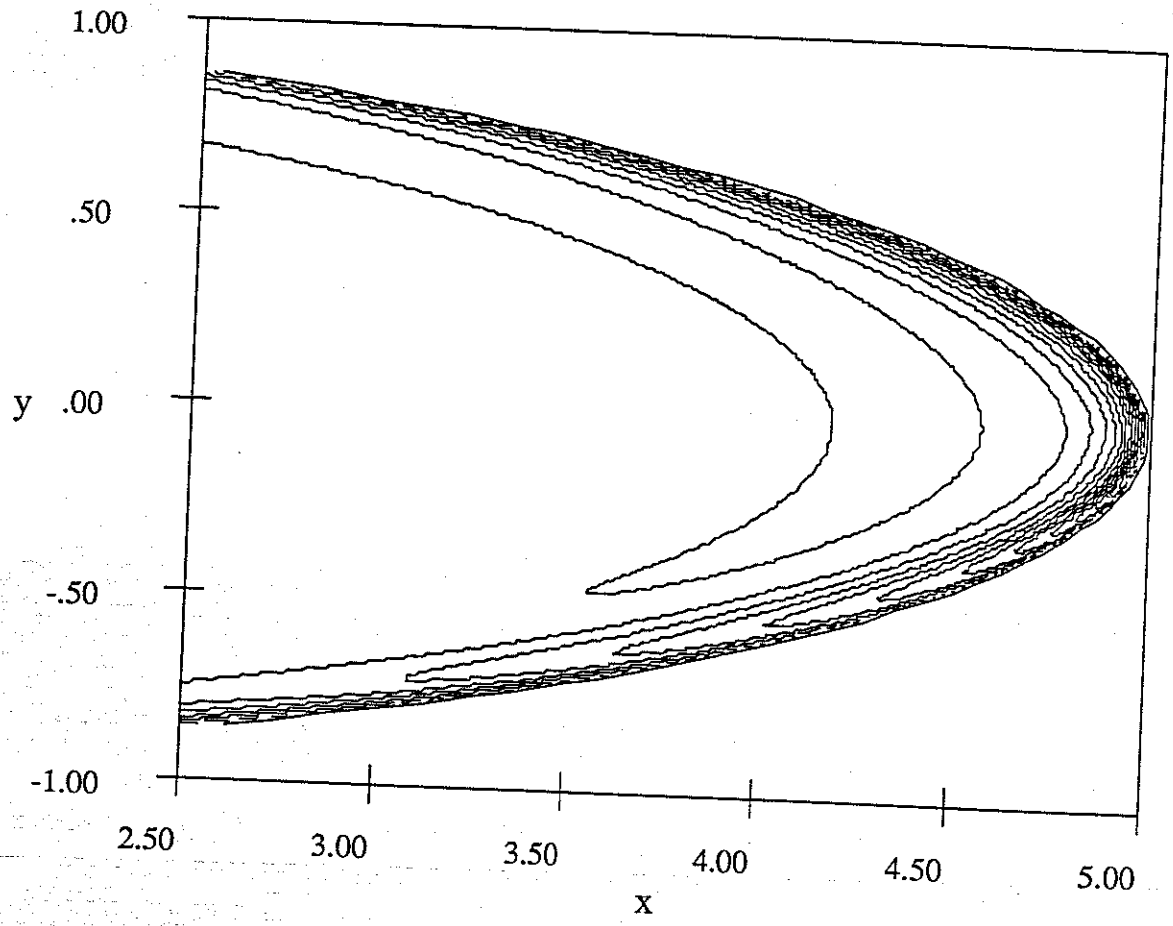
1.00
.50
y .00
-.50
-1.00
2.50
3.00
3.50
4.00
4.50
5.00
x

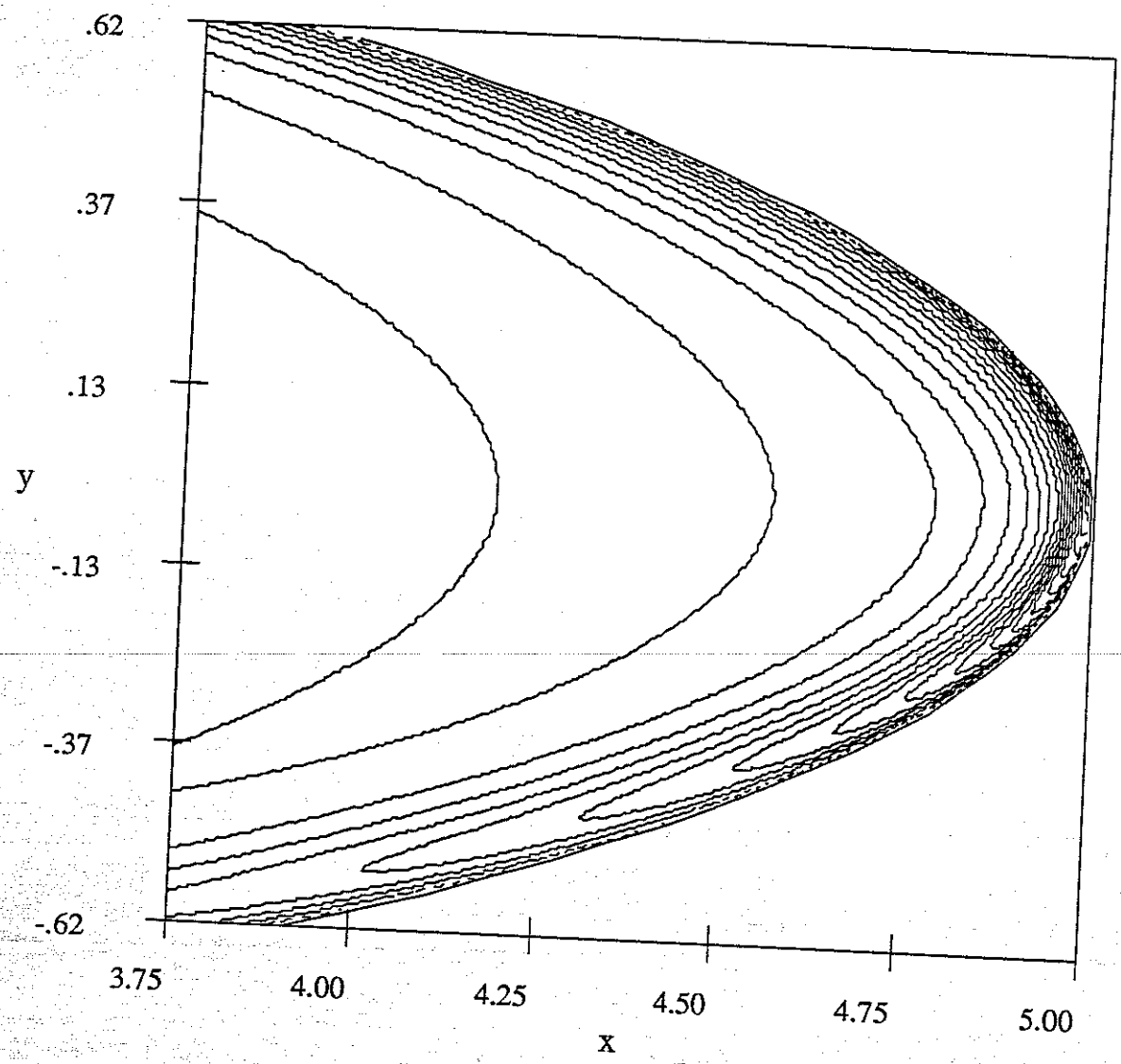
.62
.37
.13
y
-.13
-.37
-.62
3.75
4.00
4.25
4.50
4.75
5.00
x

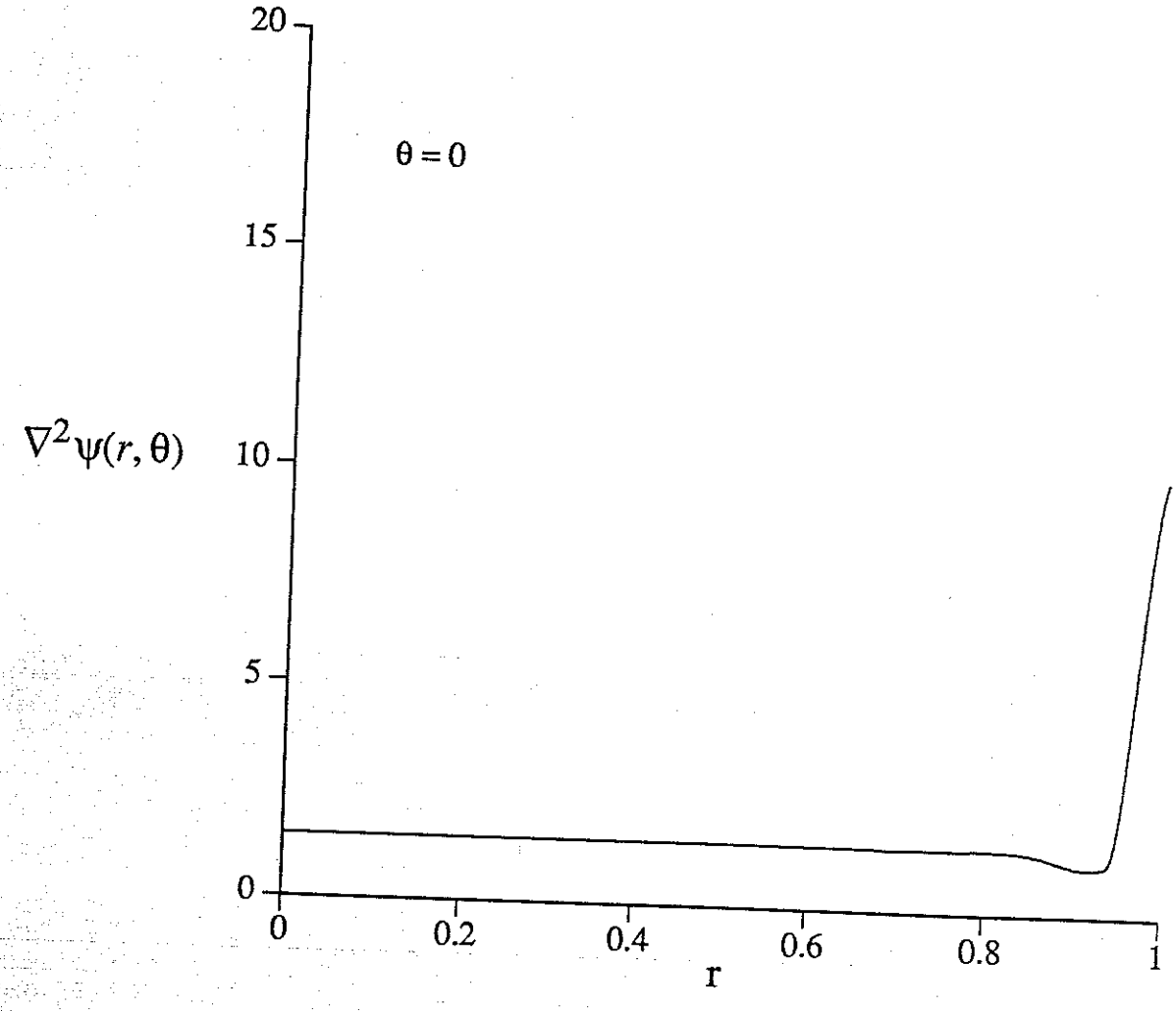
20
15
10
5
0
θ = 0
$\nabla^2\psi(r,\theta)$
0
0.2
0.4
0.6
0.8
1
r

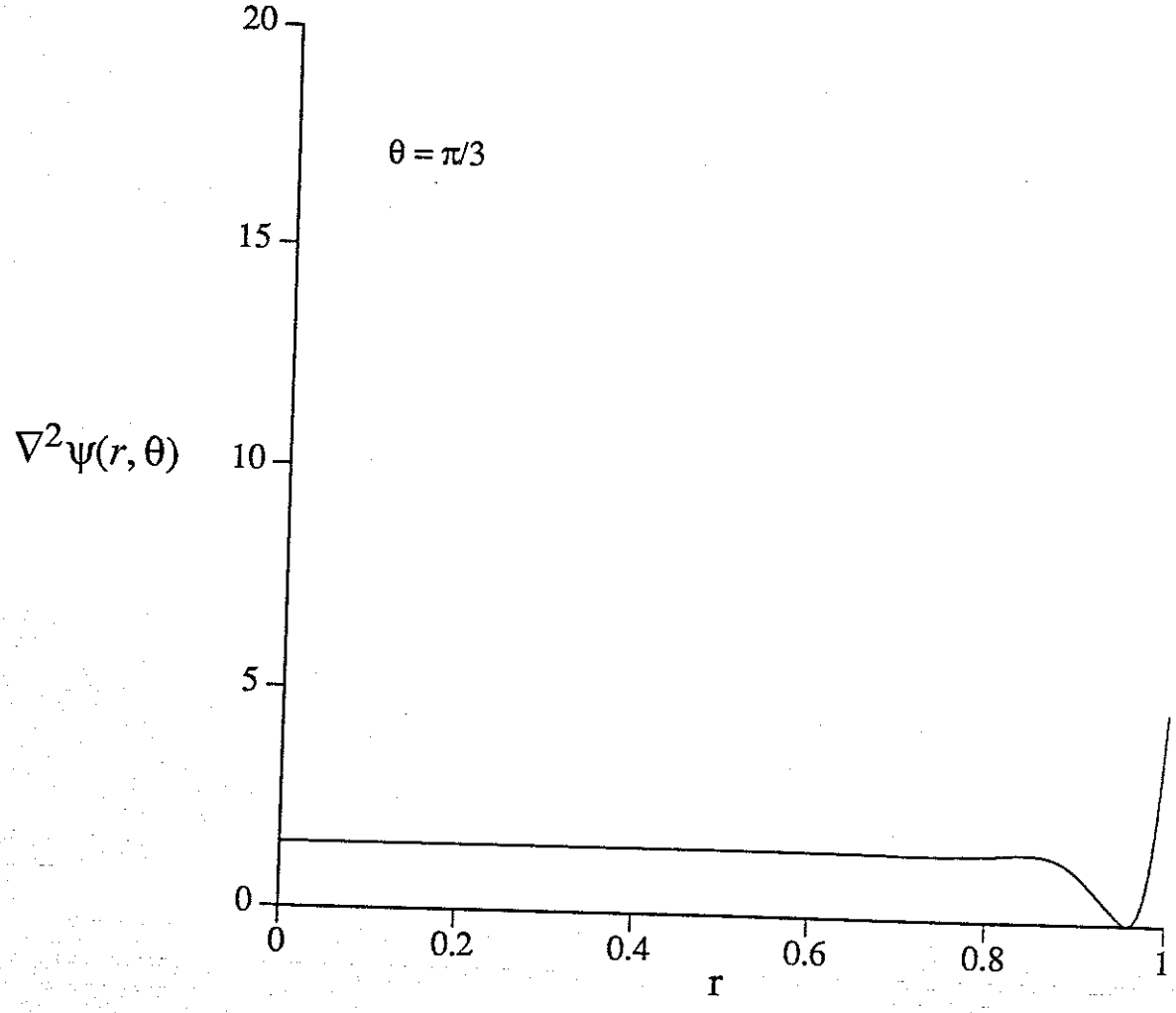
20
15
10
5
0
θ = π/3
∇²ψ(r, θ)
0
0.2
0.4
0.6
0.8
1
r

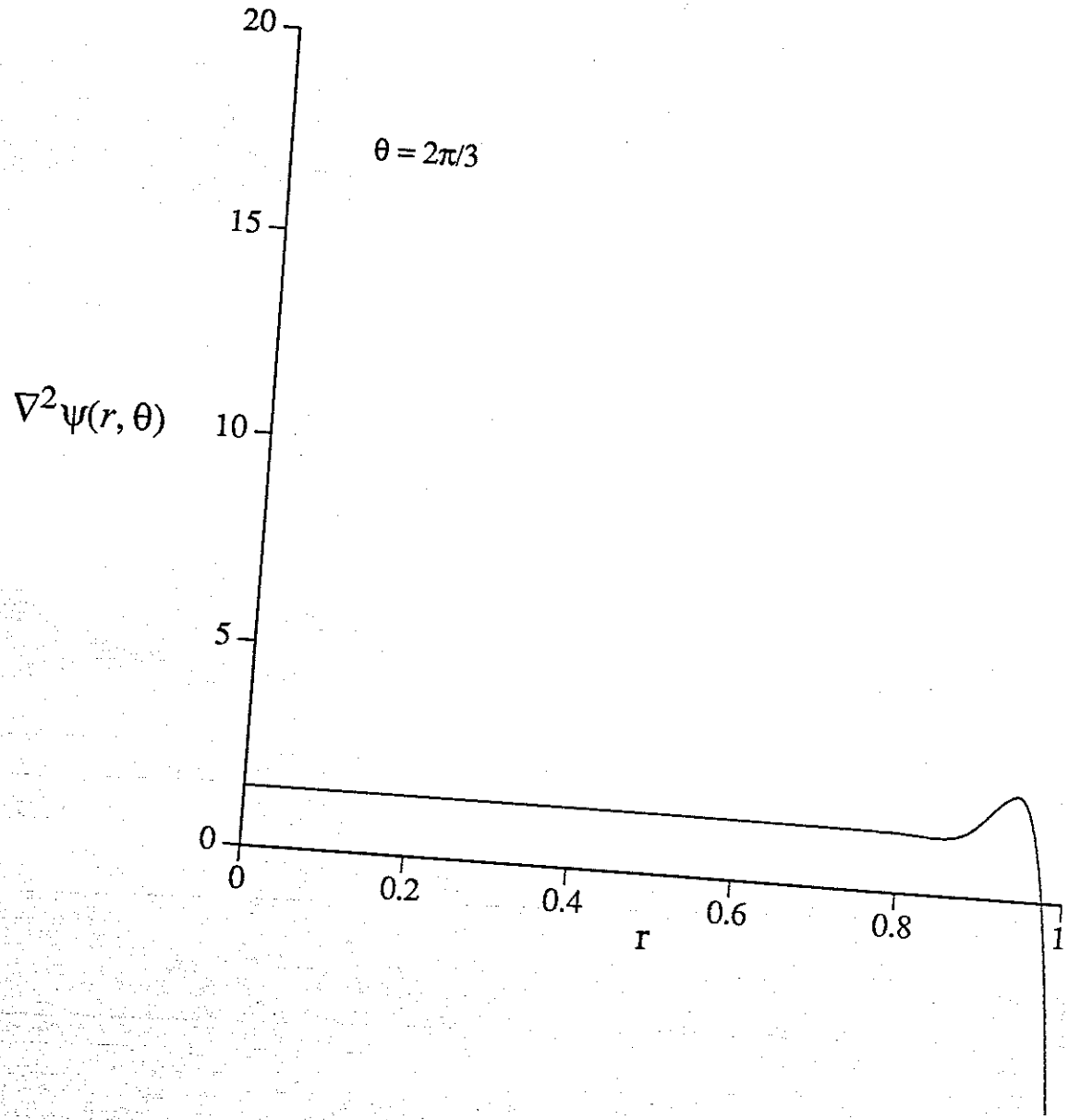
20
15
10
5
0
$\theta = 2\pi/3$
$\nabla^2\psi(r, \theta)$
0
0.2
0.4
0.6
0.8
1
r

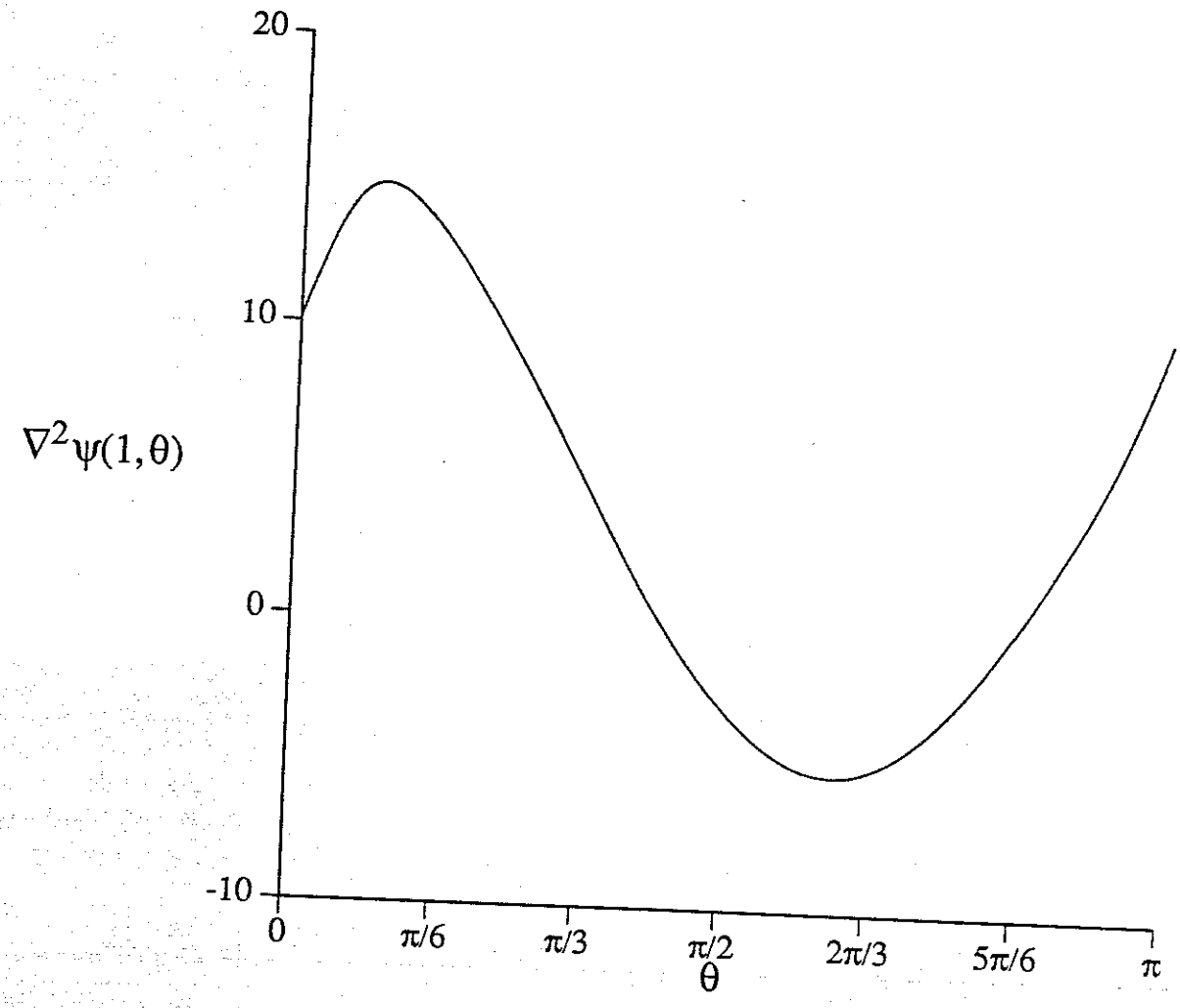
20
10
0
-10
$\nabla^2\psi(1,\theta)$
0
π/6
π/3
π/2
2π/3
5π/6
π
θ

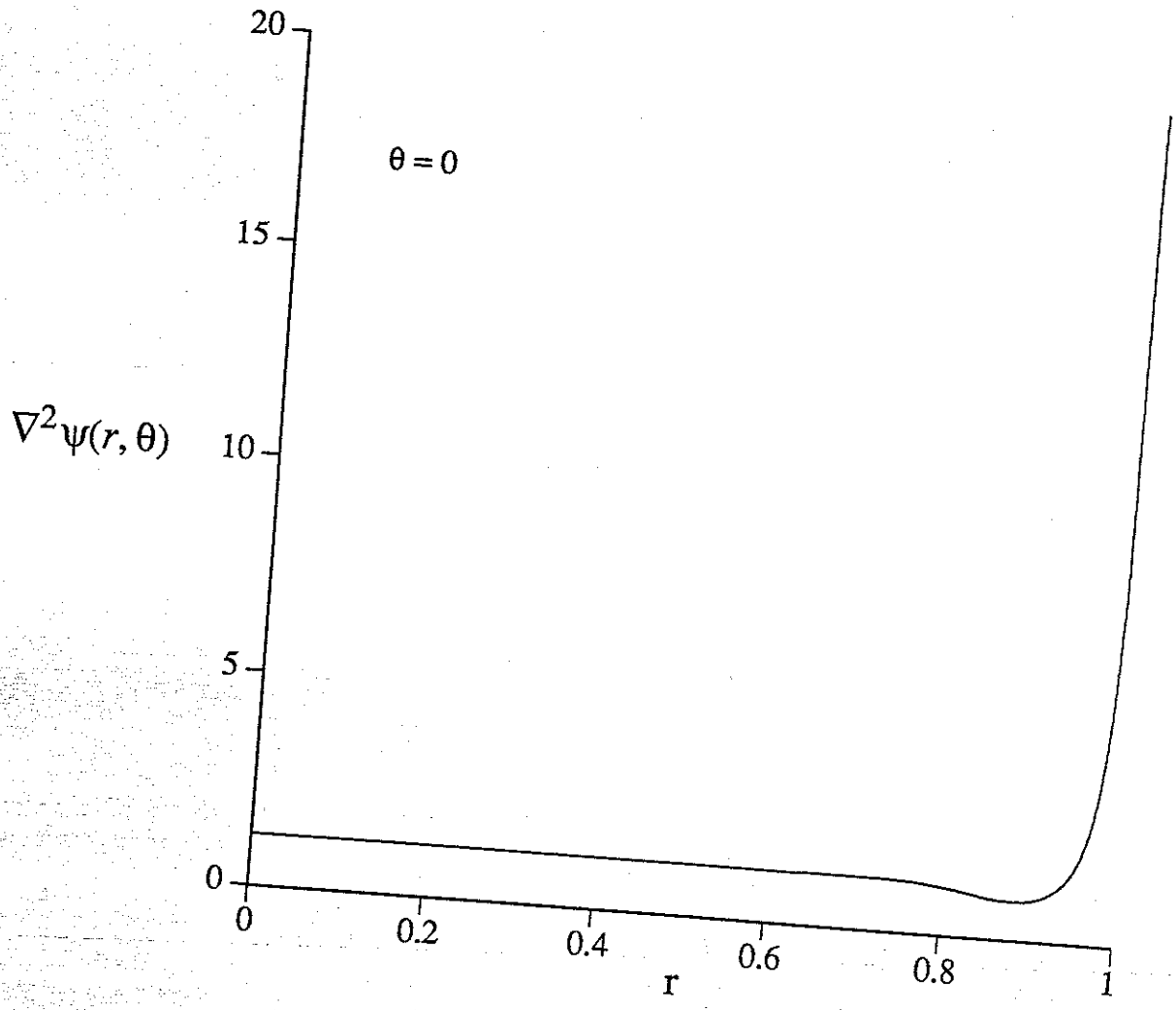
20
15
10
5
0
$\theta = 0$
$\nabla^2\psi(r, \theta)$
0
0.2
0.4
0.6
0.8
1
r

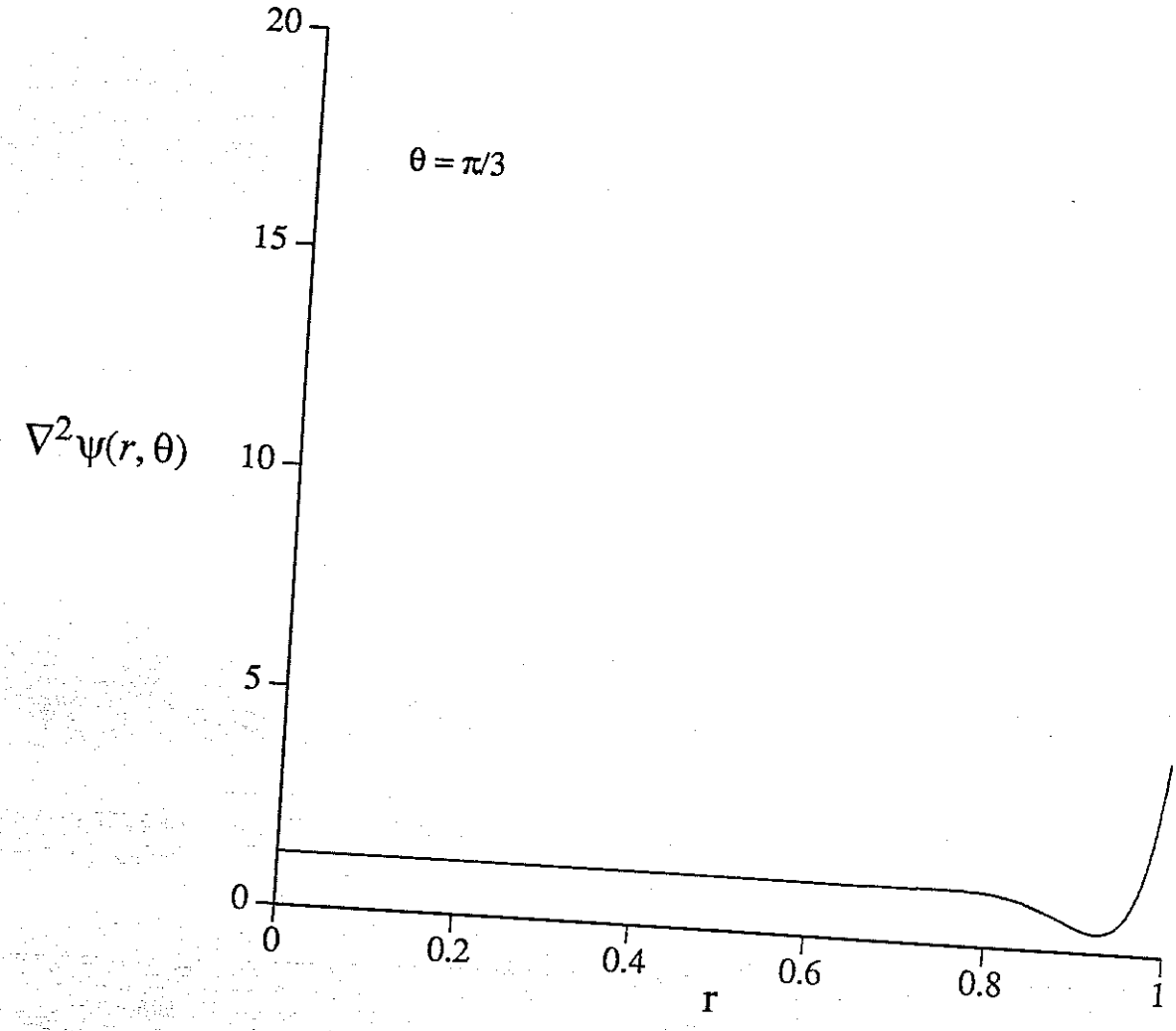
20
15
10
5
0
$\theta = \pi/3$
$\nabla^2\psi(r, \theta)$
0
0.2
0.4
0.6
0.8
1
r

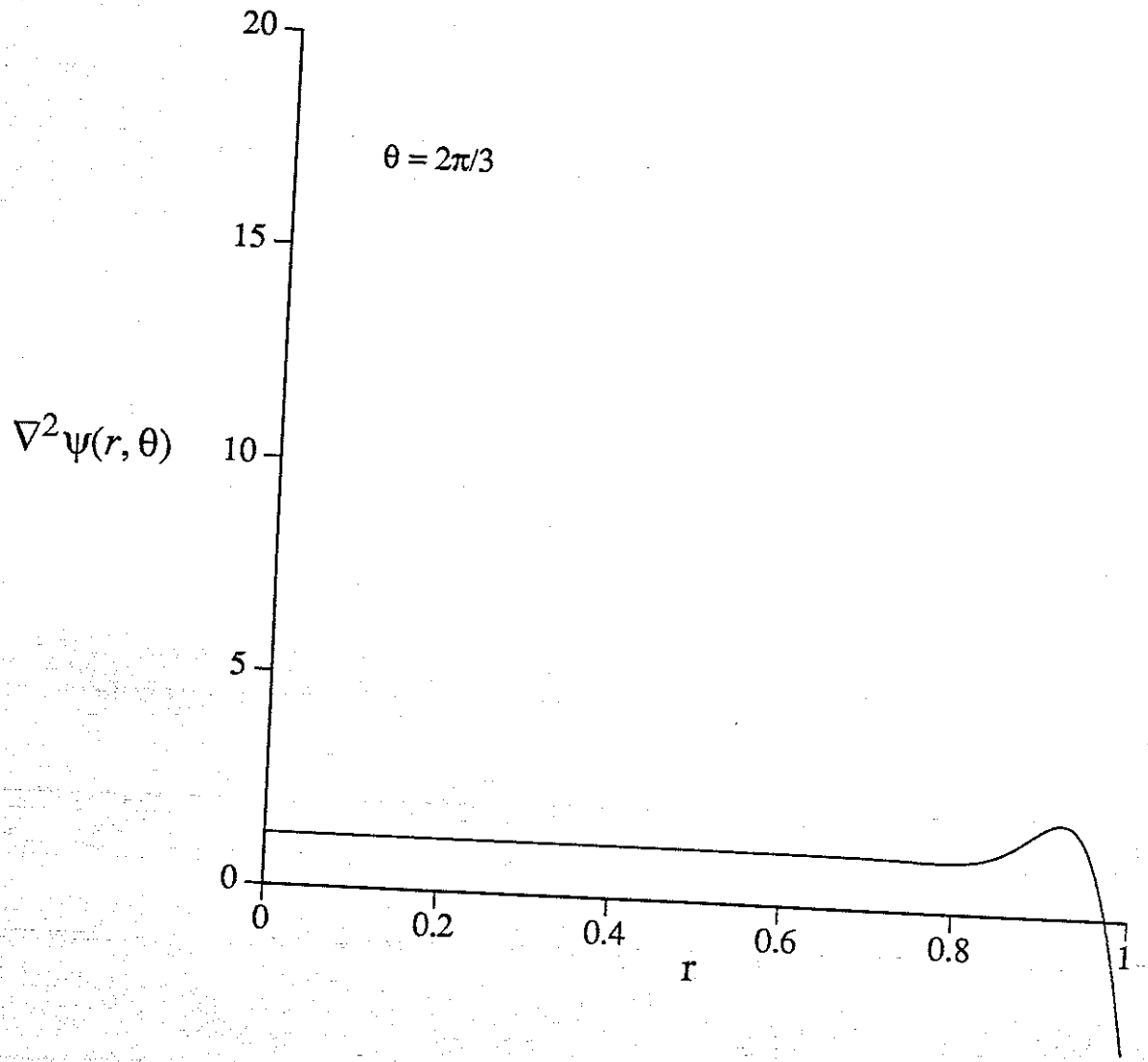
20
15
10
5
0
$\nabla^2\psi(r,\theta)$
$\theta = 2\pi/3$
0
0.2
0.4
0.6
0.8
1
r

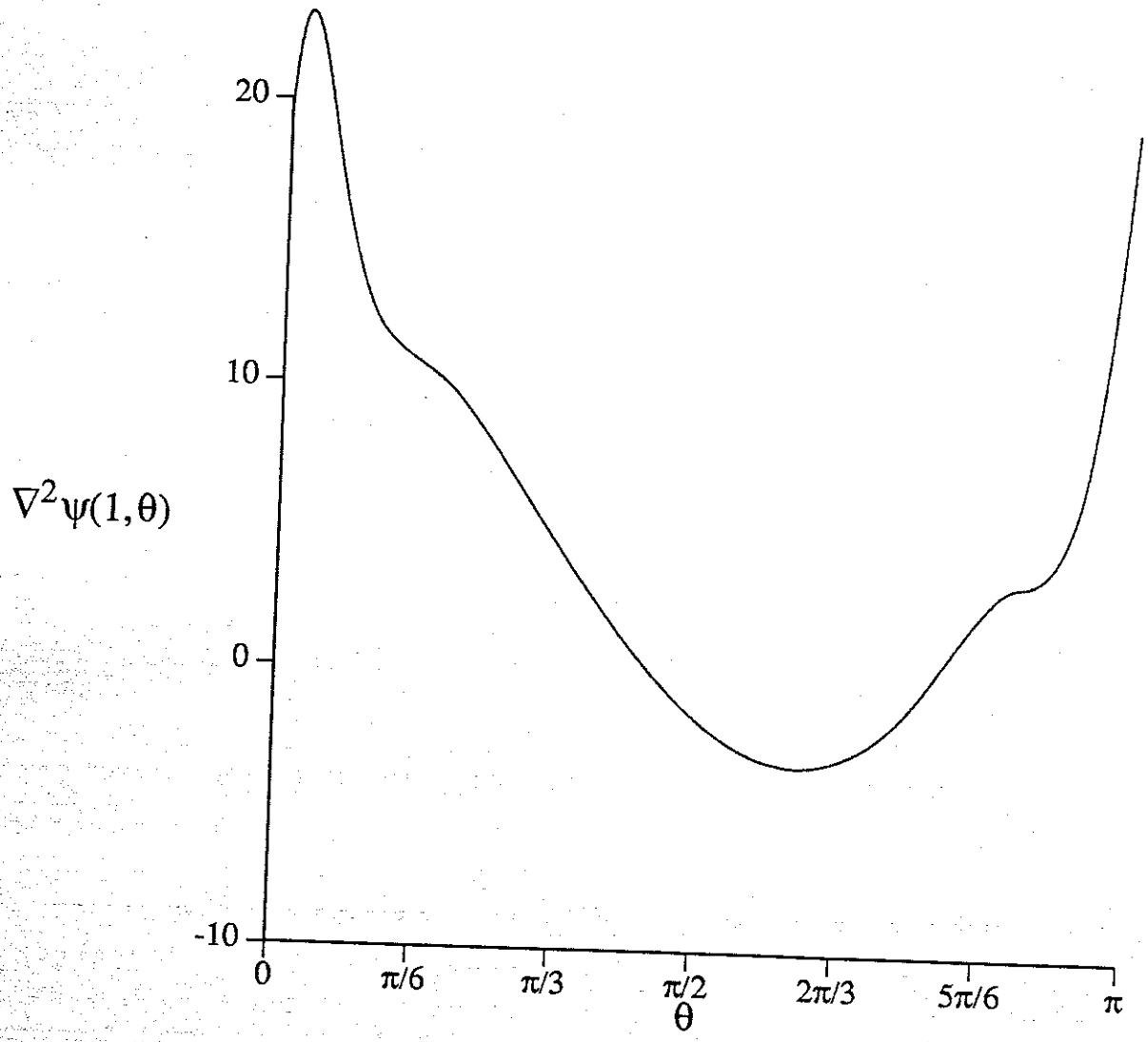
$\nabla^2\psi(1,\theta)$
20
10
0
-10
0
π/6
π/3
π/2
2π/3
5π/6
π
θ

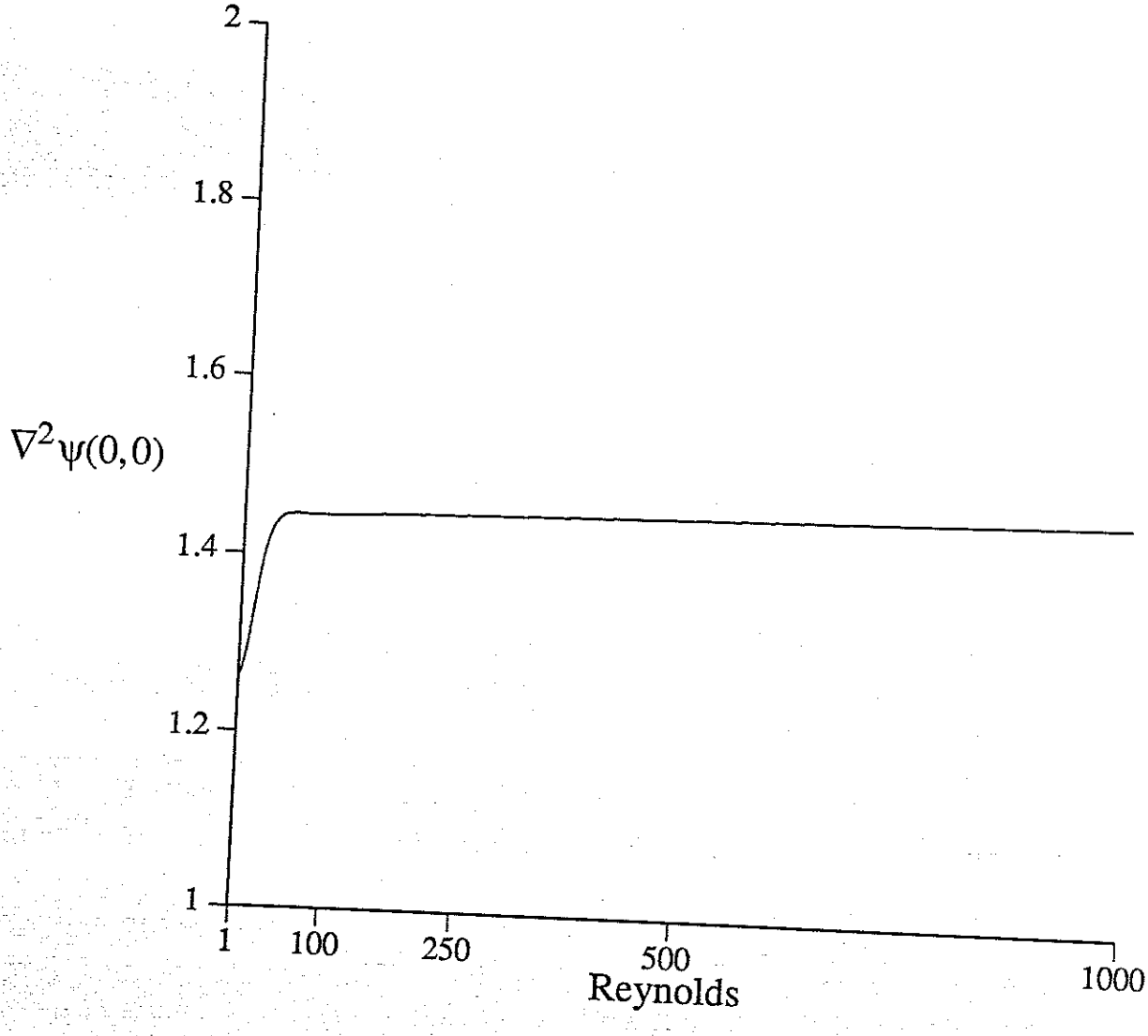
2
1.8
1.6
$\nabla^2\psi(0,0)$
1.4
1.2
1
1
100
250
500
1000
Reynolds

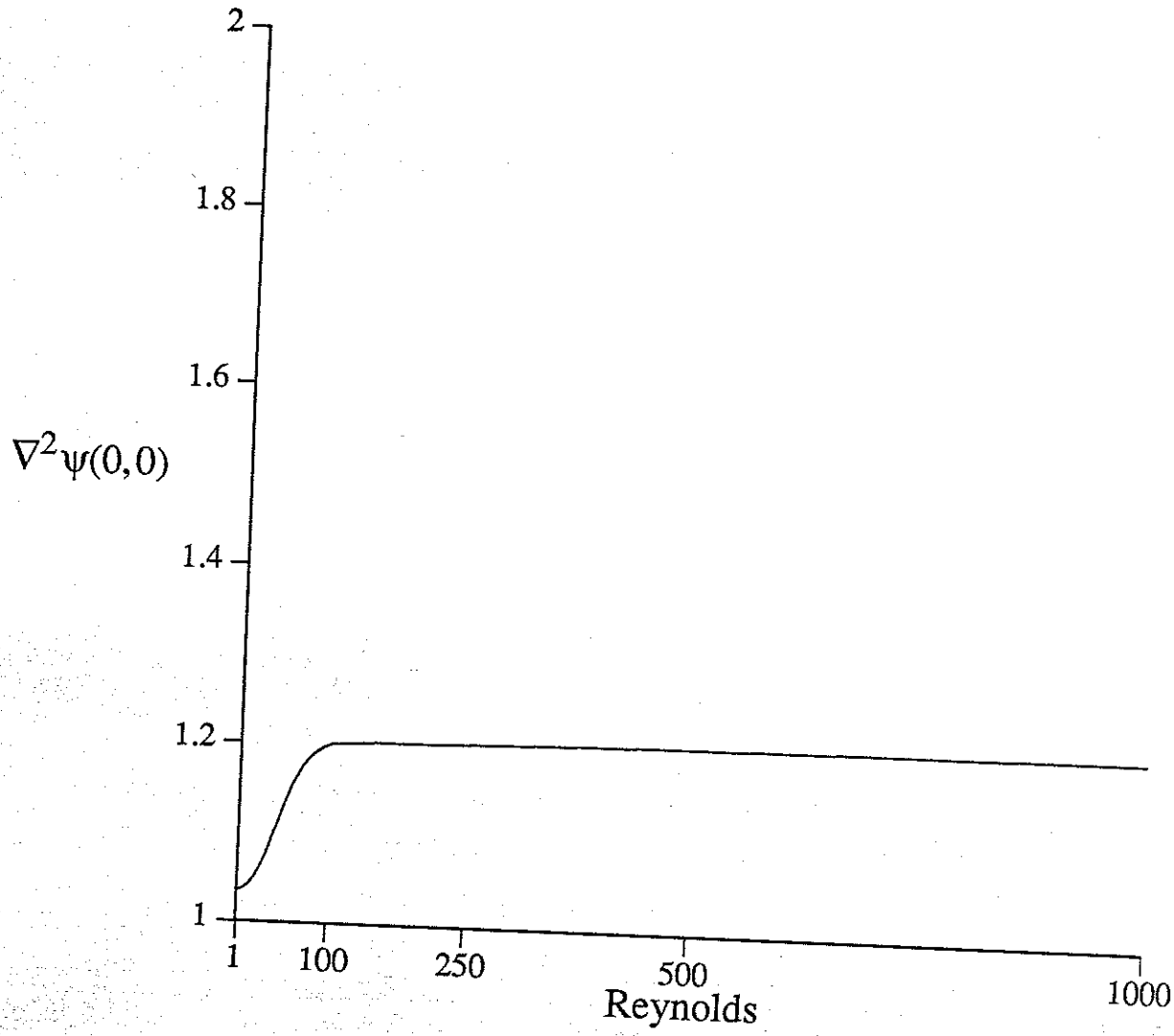
2
1.8
1.6
$\nabla^2\psi(0,0)$
1.4
1.2
1
1
100
250
500
1000
Reynolds